

CHARACTERIZATION OF NOVEL MATERIALS FOR FUSED FILAMENT
FABRICATION

A THESIS SUBMITTED TO
THE GRADUATE SCHOOL OF NATURAL AND APPLIED SCIENCES
OF
MIDDLE EAST TECHNICAL UNIVERSITY

BY

ABDULLAH ABDULRAHMAN NAJI AL-DUAIS

IN PARTIAL FULFILLMENT OF THE REQUIREMENTS
FOR
THE DEGREE OF MASTER OF SCIENCE
IN
MECHANICAL ENGINEERING

JUNE 2021

Approval of the thesis:

**CHARACTERIZATION OF NOVEL MATERIALS FOR FUSED
FILAMENT FABRICATION**

submitted by **ABDULLAH ABDULRAHMAN NAJI AL-DUAIS** in partial fulfillment of the requirements for the degree of **Master of Science in Mechanical Engineering, Middle East Technical University** by,

Prof. Dr. Halil Kalıpçılar
Dean, Graduate School of **Natural and Applied Sciences**

Prof. Dr. M. A. Sahir Arıkan
Head of Department, **Mechanical Engineering**

Assoc. Prof. Dr. Sezer Özerinç
Supervisor, **Mechanical Engineering, METU**

Assoc. Prof. Dr. Feyza Kazanç Özerinç
Co-Supervisor, **Mechanical Engineering, METU**

Examining Committee Members:

Assoc. Prof. Dr. Ulaş Yaman
Mechanical Engineering, METU

Assoc. Prof. Dr. Sezer Özerinç
Mechanical Engineering, METU

Assoc. Prof. Dr. Feyza Kazanç Özerinç
Mechanical Engineering, METU

Prof. Dr. Göknur Bayram
Chemical Engineering, METU

Asst. Prof. Dr. Evren Yasa
Mechanical Engineering, ESOGU

Date: 24.06.2021

I hereby declare that all information in this document has been obtained and presented in accordance with academic rules and ethical conduct. I also declare that, as required by these rules and conduct, I have fully cited and referenced all material and results that are not original to this work.

Name Last name: Abdullah Abdulrahman Naji Al-duais

Signature:

ABSTRACT

CHARACTERIZATION OF NOVEL MATERIALS FOR FUSED FILAMENT FABRICATION

Al-duais, Abdullah Abdulrahman Naji
Master of Science, Mechanical Engineering
Supervisor: Assoc. Prof. Dr. Sezer Özerinç
Co-Supervisor: Assoc. Prof. Dr. Feyza Kazanç Özerinç

June 2021, 77 pages

Fused filament fabrication (FFF) is a polymer additive manufacturing technology that is suitable for a wide range of applications due to its low cost and ease of use. This thesis investigated two types of novel materials for FFF use. First, a foaming PLA filament is considered and the mechanical properties of 3D printed specimens using this filament is characterized. The results show that the strength, modulus and density of the foaming PLA can be tuned over a wide range of values by varying FFF process parameters. The second part of the thesis explored the synthesis of ABS-fly ash composite filaments. 3D printing of this composite is successfully demonstrated and the mechanical properties are characterized.

Keywords: Fused Filament Fabrication (FFF), Polymer-Fly ash composite filament, Foaming polymer filament, Mechanical properties, Printing parameters.

ÖZ

ERİYİK FİLAMANT İLE İMALAT YÖNTEMİNE YÖNELİK YENİLİKÇİ MALZEMELERİN İNCELENMESİ

Al-duais, Abdullah Abdulrahman Naji
Yüksek Lisans, Makina Mühendisliği
Tez Yöneticisi: Doç. Dr. Sezer Özerinç
Ortak Tez Yöneticisi: Doç. Dr. Feyza Kazanç Özerinç

Haziran 2021, 77 sayfa

Eriyik Filament ile İmalat (EFİ), düşük maliyet ve kolay üretim özellikleri nedeniyle birçok uygulama için uygun bir eklemeli imalat yöntemidir. Bu tez kapsamında iki farklı yenilikçi filament malzemesi ele alınmıştır. İlk olarak köpüklenme kabiliyetine sahip PLA filament incelenmiştir. Bu filament ve bir 3B yazıcı kullanılarak üretilen yapıların mekanik özellikleri belirlenmiştir. Yapının dayanım, elastikiyet modülü ve yoğunluk gibi özelliklerinin EFİ üretim parametrelerine bağlı olarak geniş bir aralıkta ayarlanabildiği tespit edilmiştir. Tezin ikinci kısmında, ABS ve uçucu külden oluşan bir kompozit filament geliştirilmiştir. Bu filamentin 3B yazıcı aracılığıyla parça üretimi başarılı şekilde gerçekleştirilmiş ve üretilen yapıların mekanik özellikleri belirlenmiştir.

Anahtar Kelimeler: Eriyik Filament ile İmalat (EFİ), Polimer-uçucu kül kompozit filament, köpüren PLA filament, Mekanik özellikleri, Üretim parametreleri.

To My Mother, Sisters, Brother, and the Soul of My Father

To My Wife and Son

ACKNOWLEDGMENTS

I would like to show my great and sincere gratitude and deep appreciation to my supervisor, Assoc. Prof. Dr Sezer Ozerinc for his unlimited support, guidance, patience, advice, and encouragement throughout my master program. I also would like to sincerely thank Assoc. Prof. Dr Feyza Kazanç Özerinç and Prof. Dr Gökür Bayram for their outstanding and precious contribution to this work. A special note of thanks to all members of clean combustion technologies and polymer labs for the great help and support during the preparation of the filament used in this study.

I also would like to thank all my great friends and colleagues at the nanomechanics laboratory team for their support and encouragement throughout my research and lab work. I also want to thank all my Yemeni friends at METU, who were great companies throughout this time; thanks for their support and encouragement.

Finally, I want to express my sincere gratitude to my mother, Misk Ali, my wife, Muna Abdulwahab, and all my family for their support, patience, and encouragement. A special and sincere note of thanks and gratitude to my brother Eng. Abdulsalam, who was beside me in every single step throughout my educational journey. His unwavering support and encouragement are the reason that kept me chasing my aspirations and goals; thanks for not compromising on my education under any circumstances.

TABLE OF CONTENTS

ABSTRACT.....	v
ÖZ.....	vi
ACKNOWLEDGMENTS.....	viii
TABLE OF CONTENTS.....	ix
LIST OF TABLES.....	xii
LIST OF FIGURES.....	xiii
CHAPTERS	
1 INTRODUCTION.....	1
1.1 Fused Filament Fabrication (FFF).....	1
1.1.1 Working principle of FFF.....	3
1.1.2 FFF parameters.....	5
1.1.3 Materials.....	9
1.2 The mechanical properties of FFF-printed parts.....	11
1.3 Polymer composite for FFF.....	12
1.3.1 Fiber-reinforced polymer composite.....	13
1.3.2 Particle-reinforced polymer composite.....	14
1.3.3 Nanocomposite.....	14
2 TUNABLE MECHANICAL PROPERTIES OF FOAMING PLA PRODUCED BY FFF.....	17
2.1 Abstract.....	17
2.2 Introduction.....	18
2.3 Experimental Details.....	19

2.4	Results and Discussion	23
2.4.1	Effect of Nozzle Temperature.....	23
2.4.2	Effect of Filament Flow Rate.....	28
2.4.3	Effect of printing speed.....	31
2.4.4	Effect of infill Ratio	32
2.4.5	Effect of Layer Thickness	35
2.4.6	Compression test.....	39
2.4.7	Shore hardness measurement.....	41
2.4.8	Thermal characterization.	42
3	DEVELOPMENT OF ABS-FLY ASH COMPOSITE FILAMENTS FOR FFF	45
3.1	Abstract.....	45
3.2	Introduction	46
3.1	FA	46
3.1.1	Classification of FA	49
3.2	Characterization of FA	49
3.2.2	FA in the polymer industry	52
3.2.3	Polymer-FA composite in FFF	57
3.3	Experimental details	57
3.3.1	Pure ABS and ABS-FA Filament preparation	57
3.3.2	Mechanical testing	60
3.3.3	Surface morphology characterization	60
3.3.4	X-ray diffraction analysis	60
3.3.5	Differential scanning calorimetry and thermal gravimetric analysis.....	60

3.4	Results and discussion	61
3.4.1	XRD results	61
3.4.2	DSC and TGA results.....	61
3.4.3	Mechanical test results	63
4	CONCLUSION AND FUTURE WORK	67
	REFERENCES	69
	APPENDICES	
A.	Ashby-Gibson Model of Closed-cell Foam Structures.....	77

LIST OF TABLES

TABLES

Table 1. The bulk mechanical properties of materials used for FFF.	11
Table 2. The mechanical properties of FFF-printed parts.	12
Table 3. Printing parameters common to all specimens in LW-PLA study.	20
Table 4. The printing parameters investigated in LW-PLA study.	22
Table 5. LW-PLA Foams characterization at different flow rate (%) based on SEM images of Figure 11.	31
Table 6. DSC test results of LW-PLA.	43
Table 7. General physical properties of FA.	50
Table 8. The chemical composition of different types of FA.	51
Table 9. Polymer-FA composites.	54
Table 10. The mechanical properties of ABS.	55
Table 11. The printing parameters common to all specimens of this study.	59
Table 12. Summary of the mechanical properties of ABS and ABS-FA specimens.	65

LIST OF FIGURES

FIGURES

Figure 1. A schematic drawing of the FFF technology.....	2
Figure 2. The publication number appears in the SCOPUS search engine regarding the mechanical properties related to the FFF-printed parts to be searched within the article title, abstract, and keywords.....	3
Figure 3. Data Processing in FFF.	4
Figure 4. Different air gaps configuration, (a) positive, (b) zero, and (c) negative..	6
Figure 5. Different configurations of raster orientation, top view of 3D printer.	8
Figure 6. Schematic views of the specimen geometries. (a) Tensile specimen with a thickness of 3.2 mm, (b) compression specimen, (c) graded specimen for shore hardness measurements. All dimensions are in mm.	20
Figure 7. The stress-strain curves for specimens printed at different nozzle temperatures.	23
Figure 8. (a) The tensile strength and elastic modulus, (b) the elongation at break, (c) the density, and (d) the specific properties of the printed specimens at different nozzle temperatures. The error bar represents one standard deviation obtained from testing three samples. The error bar at 260 °C Figure (a) is very small to be shown.	26
Figure 9. Optical microscope images of the printed specimens as a function of nozzle temperature.	27
Figure 10. (a) The tensile strength and modulus, (b) the elongation at break, (c) the density, and (d) the specific tensile strength and modulus of the printed specimens at different flow rates at two nozzle temperatures at 230 and 245 °C.	29
Figure 11. Cross-section SEM images of 3D-printed samples with a variable flow rate of (a) 100 %, (b) 50 %, (c) and 25 %.....	30
Figure 12. (a) The tensile strength and elastic modulus, (b) the elongation at break, (c) the density, and (d) the specific tensile strength and modulus of the printed specimens at different printing speeds at two sets of nozzle temperature.	32

Figure 13. (a) The tensile strength and elastic modulus, (b) the elongation at break, (c) the density, (d) the specific properties, and (e) the image of the specimens printed specimens at different infill ratios.	34
Figure 14. The densities of specimens printed at different layer thicknesses.	35
Figure 15. (a) The tensile strength - density, (b) the elastic modulus - density, (c) the specific strength - density, and (d) the specific strength - the elastic modulus figures of all specimens printed at different printing parameters.	36
Figure 16. (a) The tensile strength - density, and (b) the elastic modulus - density figures of all specimens printed at different printing parameters calculated experimentally and theoretically according to Gibson-Ashby model.	38
Figure 17. (a) The compressive stress-strain curves, (b) the compressive strength and modulus, and (c) the specific modulus and densities.	40
Figure 18. The image of compression specimens printed at different flow rates (%).	41
Figure 19. The shore hardness at a different flow rate. The error bar represents one standard deviation obtained from measuring five different points.	41
Figure 20. (a) The DSC of the filament and specimens printed at different nozzle temperature, heat flow endu up, and (b) the TGA of the filament used.	44
Figure 21. FA generation and collection in a pulverized coal-fired power plant (Adapted from (Chou 2012)).	47
Figure 22. FA production and utilization (million tones (MT) /year) in different countries.	48
Figure 23. (a) SEM image of the FA used in this study and (b) particle size distribution histogram.	58
Figure 24. (a) Dimensions of the tensile specimen. The specimen thickness is 3.2 mm. (b) Photographs of tested specimens of the pure ABS (white) and the ABS-FA (grey).	59
Figure 25. XRD spectrum of pure ABS and ABS-FA composite specimens.	61
Figure 26. (a) DSC data of ABS and ABS-FA. (b) TGA data of ABS and ABS-FA.	62

Figure 27. The stress-strain curves for the ABS (blue) and ABS-FA (red) specimens..... 64

Figure 28. SEM images of the fracture surface of the ABS-FA specimen. (a) and (b) show two different regions of the same surface at different magnifications..... 65

CHAPTER 1

INTRODUCTION

1.1 Fused Filament Fabrication (FFF)

The increasing demand for manufacturing high-quality products with low cost have increased the competition among the different manufacturing societies. Researchers worldwide seek to provide advanced technologies that can produce complex parts fast, neatly and costly-efficient. On the other hand, to develop existing products to serve a specific purpose, prototypes of the product's solid model should be first created to examine their final properties, known as rapid prototyping (RP) or 3D printing. Additive manufacturing (AM) is another name for 3D printing since it works according to the building of the physical model by selectively adding material as thin layers. Many AM technologies now are available, like FFF, stereolithography (SL), selective laser sintering (SLS), selective laser melting (SLM), laminated object manufacturing (LOM), and others (Fountas and Vaxevanidis 2021).

FFF is one of the most used kinds of AM, particularly for polymers. It has the ability to fabricate very complex parts efficiently at a low cost; Figure 1 shows a schematic drawing of the main parts of this technology. Furthermore, FFF can be used efficiently for prototyping applications since no mold preparation or solvent is needed; it has also been widely used for custom fabrication (Zein et al. 2002).

Here are some of the most applicable areas for FFF (Chartier and Badev 2013),

- Fast and cost-efficiently fabrication of early-stage prototypes of product development or end-use parts to be integrated immediately on a system.
- The fabrication of prototypes with specific characteristics to be tested in a real-world environment.

- Cost-efficiently fabrication of some manufacturing tools like fixtures or jigs, and
- Custom fabrications such as games or souvenirs, usually done by the hobbyist.

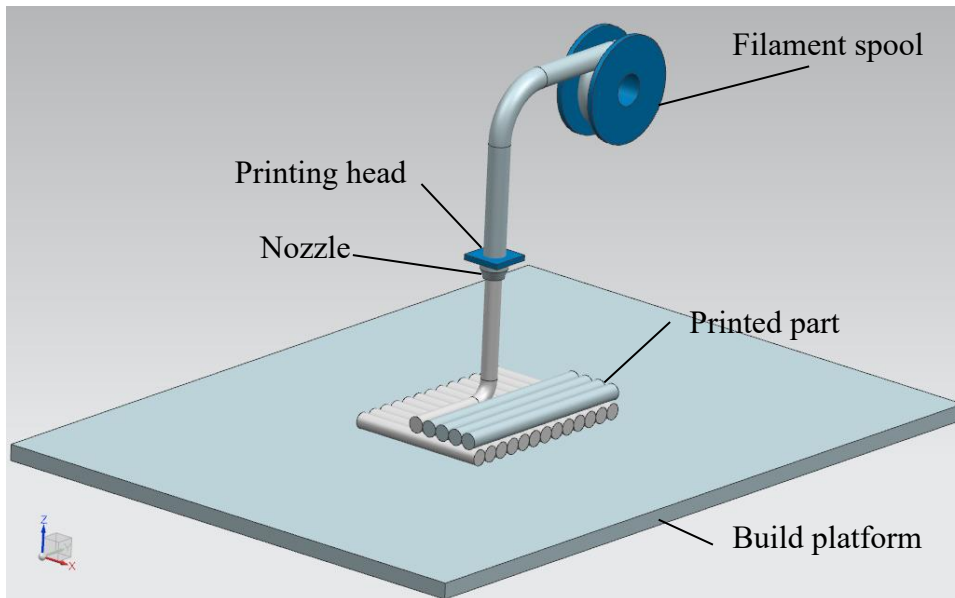


Figure 1. A schematic drawing of the FFF technology.

In 2020 the number of publications on the FFF-printed parts' mechanical properties (386) had increased by 600% compared to those publications in 2015 (55), Figure 2. This sharp increase in research and publications has proved the great importance of FFF in manufacturing societies; it also provides more comprehensive data for the best mechanical performance.

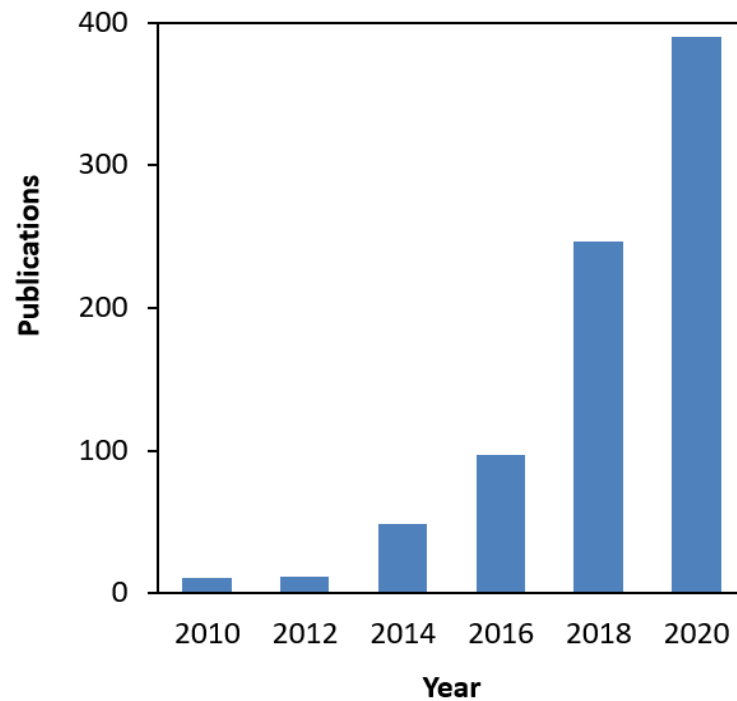


Figure 2. The publication number appears in the SCOPUS search engine regarding the mechanical properties related to the FFF-printed parts to be searched within the article title, abstract, and keywords.

1.1.1 Working principle of FFF

In FFF, the desired part to be printed is first designed as a 3D model by any CAD package program, then exported as a stereolithography (STL) file to a slicing program like Simplify 3D or Cura. The slicing program then formulates, in G-code format, a processing plan to guide the 3D printing machine during the entire printing process, Figure 3.

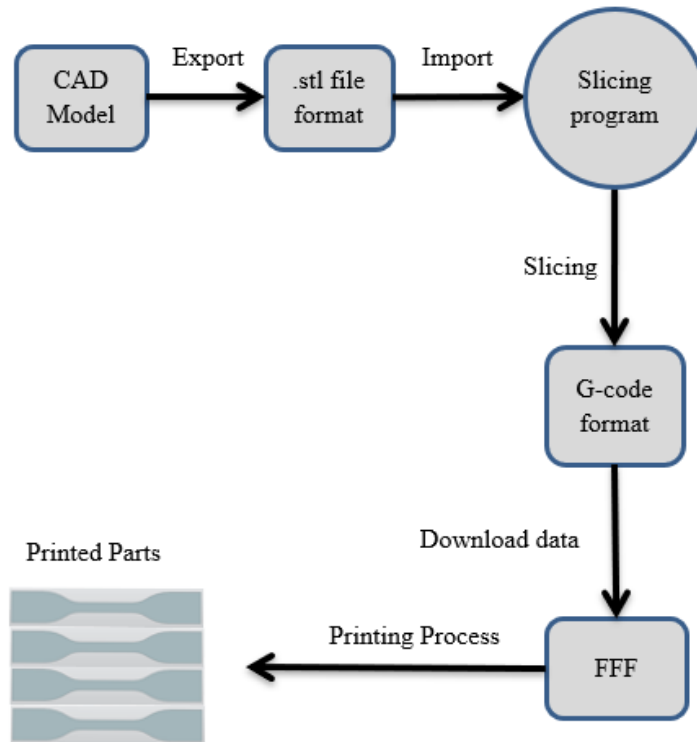


Figure 3. Data Processing in FFF.

The fabrication of the parts then starts first by melting the polymer material into a liquid state. After that, the material, which is in a molten state, is extruded as a thin filament through a controlled nozzle, moves in the X-Y plane, into a table, moves in the Z direction, where it solidifies. The bonding between the neighbouring fibres then is occurring due to the partial melting of the existing fiber upon contact with the incoming hot fiber to form a layer. Then, the plate moves in the Z direction to repeat the same deposition process for printing the next layer. Finally, the successive layers fuse to build the part layer by layer (Abeykoon, Sri-Amphorn, and Fernando 2020; Wimpenny, Pandey, and Kumar 2017).

1.1.2 FFF parameters

Several parameters affect the final properties of the FFF-printed parts, and I will discuss only those parameters that are completely relying on the processing parameters. These parameters are the most investigated.

1.1.2.1 The nozzle temperature

Nozzle temperature is the temperature causing the melting of the polymer during the printing process. It has been considered one of the most critical parameters that significantly affect the printed parts' final properties. Nozzle temperature affects the printed parts' microstructure; it also changes the crystallization level, which can influence the final properties of the printed parts (Bakır, Atik, and Özerinç 2021a; Kaygusuz and Özerinç 2019).

At low temperature, several studies have shown that the filament material will not melt properly for providing the required viscosity for strong bonding between the neighbouring fibers from one side and between the successive layers from the other side. However, the higher the nozzle temperature is, the more time is required for the melt material for cooling; such a delay in time affects the final parts' crystallinity and, consequently, the final properties. Furthermore, at high nozzle temperature, the melted material's overflow will increase the fusion between the adjacent fibers and layers. However, it will affect the printed parts' dimensional stability since neighbouring fibers or layers will overlap each other, weakening the printed parts' final properties (Abeykoon et al. 2020).

1.1.2.2 The flow rate (%)

This parameter is also called the feed rate, and it describes the amount of material extruded from the nozzle per unit of time. This parameter is crucial for fabricating

lightweight products; however, some of the final properties will be compromised at a low flow rate, especially strength properties.

1.1.2.3 The infill ratio (%)

This parameter controls the gap between the neighbouring fibers. While fabricating by FFF, manufacturers usually tend to use a low infill ratio to save time and material. However, this gap will increase during a low infill ratio, leading to a faster failure of the printed parts at a low load level; those gaps act as stress concentration areas and deteriorate the printed parts' final properties.

This gap can be divided into three categories (Ahn et al. 2002),

- Positive air gap: this type saves more material; however, the bonding between the neighbouring fibers is weak and greatly affects the final properties of the printed parts. The concept of Ashby-Gibson of cellular structure can apply in this type, Figure 4 (a).
- Zero air gap: this type is considered the ideal air gap since it provides a good dimension accuracy with acceptable strength properties, Figure 4 (b).
- Negative air gap: this type makes the printed parts denser and more strength; however, negative air gaps with higher values could decrease the dimensional accuracy, Figure 4 (c).

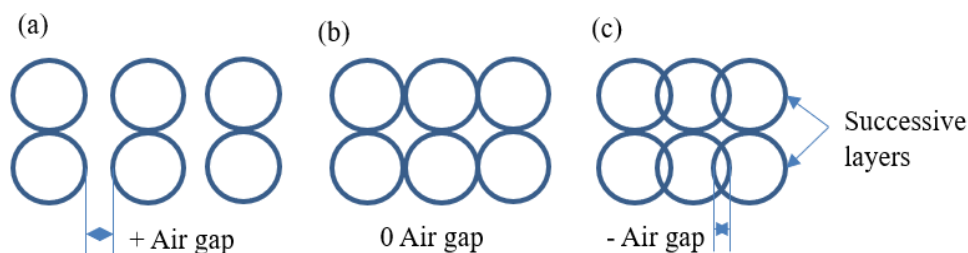


Figure 4. Different air gaps configuration, (a) positive, (b) zero, and (c) negative.

1.1.2.4 The layer thickness

Layer thickness is defined as the distance travelled in the z-direction between the adjacent layers. This parameter has more effect on the surface properties and printing time. The surface roughness level increases with increasing the layer thickness; however, less time will be used for the fabrication process. On the other hand, printing with a small layer thickness will lead to a better 3D-printed surface quality with consuming more printing time (Ayrilmis 2018; Wimpenny et al. 2017).

1.1.2.5 The raster orientation

Raster orientation represents the direction of the extruded filaments according to the axis of the loading. This parameter is critical for evaluating the printed parts' mechanical properties, Figure 5 (Ahn et al. 2002; Liu, Lei, and Xing 2019). In general, there are three main raster orientations,

- Axial raster orientation, 0° with respect to the axis of loading: specimens printed with this kind of orientation exhibit good strength properties since the loading will be along the fibers; however, stress concentration will present in the neck region where the vertical roads terminate.
- Vertical raster orientation, 90° with respect to the axis of loading: specimens printed with this kind of orientation usually exhibit weak strength properties since the loading will be between the bonding between the fibers, which is somehow weak.
- 45° or -45° raster orientation: specimens printed with this kind of orientation usually exhibit acceptable strength properties and avoid the axial specimens' stress concentration.

Furthermore, several studies have also used a combination of two kinds of rasters for better isotropic behaviour.

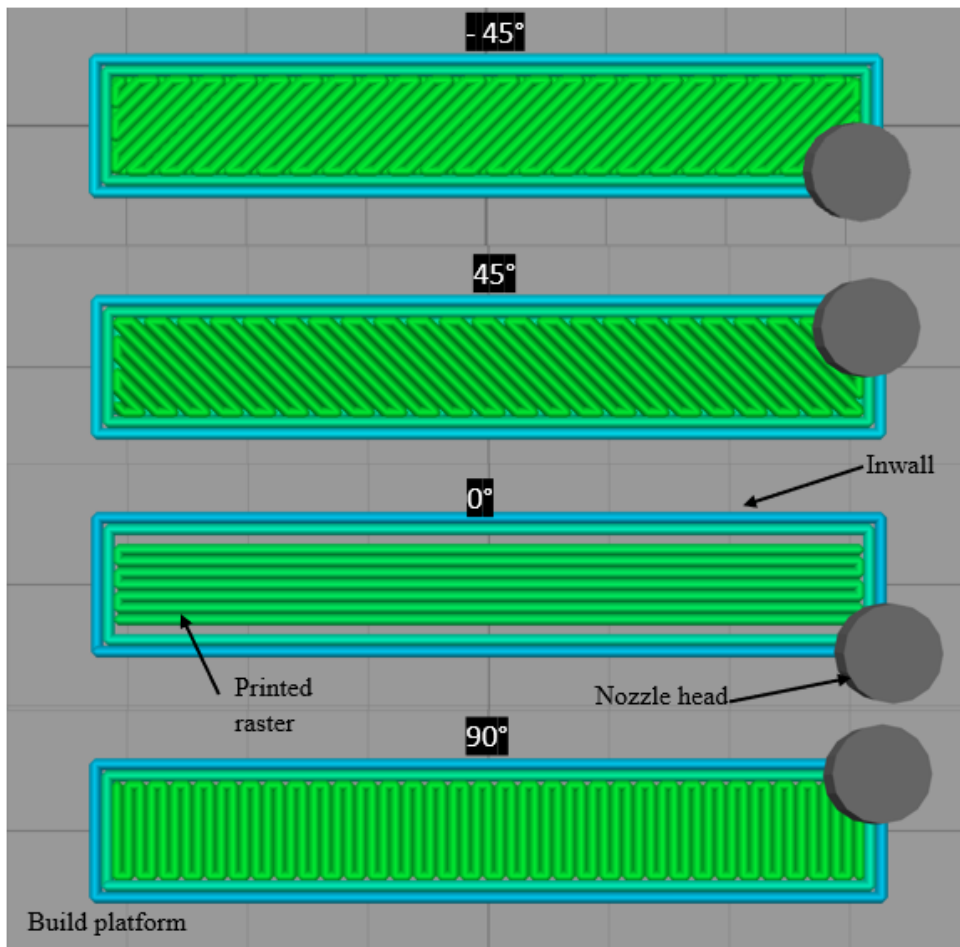


Figure 5. Different configurations of raster orientation, top view of 3D printer.

1.1.2.6 The printing speed

This parameter is defined as the nozzle speed in any direction during printing. High printing speed cause poor melting properties of the filament extruded, which leads to poor adhesion between neighbouring fibers and affects the final properties of the printed parts. On the other hand, with low printing speed, the diameter of the extruded filament will not be even and eventually affects the adhesion between the neighbouring fibers; for that reason, manufacturers usually use 50-70 mm/s printing speed (Abeykoon et al. 2020; Deng et al. 2018).

Many other parameters slightly affect the printed parts' final properties like infill pattern, bed temperature, top and bottom layer, building orientation, etc. All these parameters should be in good agreement for better final properties of the printed parts.

1.1.3 Materials

One of the most powerful advantages of FFF is the wide range of thermoplastic materials that it can handle. Polylactic acid (PLA) and acrylonitrile butadiene styrene (ABS) are the most extensively researched thermoplastics for FFF. On the other hand, many other thermoplastics have been used for FFF like nylon 6, thermoplastic polyurethane (TPU), high-density polyethylene (HDPE), polyethylene terephthalate (PET), and high-performance thermoplastics like polyether ether ketone (PEEK). PLA and ABS are the most used polymers for FFF; most of the studies related to FFF is considering PLA, ABS, or their composite; therefore I will discuss these two polymers more comprehensively.

1.1.3.1 PLA

Polylactic acid (PLA) is one of the most polymers used for FFF. The high biocompatibility and biodegradability of PLA make it a great candidate for medical

and packaging products. Furthermore, PLA is an environmentally-friendly thermoplastic, driven from renewable resources, that can be used as an alternative to many widely-used petrochemical-based plastics (Garlotta 2001; Lim, Auras, and Rubino 2008). There are three different types of PLA regarding the stereoisomers that are forming the PLA, namely poly (D-lactide) (PDLA), poly (L-lactide) (PLLA), and poly (DL-lactide). PLA enjoys high strength and modulus properties. However, the extremely low elongation at break of PLA still the main drawback that limits its usage. In general, the final mechanical properties of PLA can vary according to its component isomers and thermal history (Farah, Anderson, and Langer 2016).

1.1.3.2 ABS

Acrylonitrile butadiene styrene (ABS) is an amorphous thermoplastic polymer that has been formed by the condensation polymerization, at different proportions, of three different materials acrylonitrile, butadiene, and styrene. The final properties of the ABS depend on the proportions of the three materials mentioned above, and with a good combination of these items, it is possible to get an ABS version with some advanced characteristics. ABS gets its strength from the acrylonitrile and its ductility from butadiene elements; on the other hand, ABS's rigidity comes from the styrene elements. ABS can be manufactured by different methods like injection molding, blow molding, or extrusion processes. ABS has a low glass transition temperature of 105 °C, which make it a good choice for FFF. ABS is widely used in the electronic and automobile industries. ABS enjoys excellent properties like high toughness and rigidity, high dimensional stability, good chemical resistance, good impact resistance, good insulating characteristics, and easy processing properties. However, some drawbacks hinder its usage, like inherent flammability, low mechanical strength, very sensitivity to environmental conditions, poor weathering resistance properties, scratches easily, and low dielectric strength properties (Dromel and Singh 2021; de Oliveira et al. 2018; Olivera et al. 2016; Omnexus n.d.; Wu and Li 2014).

Table 1 shows the bulk mechanical properties of the most common materials used for FFF (Wypych 2016).

Table 1. The bulk mechanical properties of materials used for FFF.

Polymer	Elastic Modulus (GPa)	Yield Strength (MPa)	Tensile Strength (MPa)	Elongation at Break (%)
ABS	1.9-2.7	35-58	25-65	8-20
PLA	2.7-16	66-77	52-72	4-6
Nylon 6	0.78-3.6	36-95	74-106	10-160
HDPE	0.5-1.1	21-31	13-51	250-1200
TPU	0.12-0.33	39-54	17-66	300-1500
PEEK	3.5-4.4	65-95	75-100	20-50

1.2 The mechanical properties of FFF-printed parts

The printing parameters greatly affect the final mechanical properties of the FFF-printed parts. Selecting the right configuration of printing parameters is still the most challenging issue that concerns the researcher worldwide. Parts made from the same material and sharing the same geometry but different sets of printing parameters will have completely different mechanical properties. Anisotropic behaviour of FFF-printed parts is another issue that concerns the FFF society. FFF-printed parts with 0° raster orientation enjoy strength properties three times more than those of parts printed at 90° orientations (Ahn et al. 2002). This anisotropic behaviour in the strength properties due to the difference in printing orientation is critical; FFF-printed parts will experience a fast failure at low load if they are subjected to a load acting perpendicular to the raster orientation. Such a fast failure could restrict more the feasibility of using FFF-printed parts, particularly for undefined load conditions applications. Therefore, researchers usually tend to use different orientations to print the same part to decrease FFF-printed parts' anisotropic behaviour.

Table 2 shows the mechanical properties of the FFF-printed parts (Bakır, Atik, and Özerinç 2021b; Bakır et al. 2021a; Banjanin et al. 2018; Guessasma, Belhabib, and Nouri 2021; Wampol 2018). In general, FFF-printed parts' strength properties are lower than those of other parts fabricated by different conventional methods. One reason that justifies this reduction is the weak points that appear between the layers of the FFF-printed parts; those points work as a stress concentration and reduce the printed parts' strength properties. On the other hand, the wide range of the values of the FFF-printed's mechanical properties found in the literature review, Table 2, justify the aforementioned statement about the great effect of the printing parameters on the final properties.

Table 2. The mechanical properties of FFF-printed parts.

Polymer	Elastic Modulus (GPa)	Tensile Strength (MPa)	Elongation at Break (%)
ABS	1.5-2.2	2.6-53	2.1-8.6
PLA	2.7-16	13.2-66.5	4-6
Nylon 66	0.8-1.42	11.5-19	62-74
HDPE	0.9	20.2	–
rTPU	0.7-1.73	14.2-47.7	1.4-199
PEEK	0.36-4	9.3-99	2.9-111

1.3 Polymer composite for FFF

Intrinsically, the use of pure polymer filaments for FFF is limited to their mechanical properties. Most of the applications required FFF-printed parts with superior final mechanical properties that pure polymer filaments cannot provide. Composite polymer filament for FFF has addressed the previous problem efficiently and make

the possibility of shifting FFF from prototyping application to producing functional parts used in different load-bearing applications.

Polymer composite is defined as the incorporation of fibers or particles into the polymer matrix to provide the strength and stiffness required for the FFF-printed parts. Regarding its constituents, the composite polymer contains two or more different phases; first, the matrix phase, which is the primary phase that enjoys continuous characters and holds the other phase, the dispersed phase. The dispersed phase is reinforced in the primary phase in a discontinuous manner to ensure better stress transfer between the two phases. Except for PLA, the matrix phase usually enjoys high ductility with low strength properties. On the other hand, the dispersed phase enjoys higher strength properties and known as the reinforcing phase. Eventually, as a result of the combinations of the composite constituents, its final mechanical properties will be different from those of any of its constituents (Wang et al. 2017).

1.3.1 Fiber-reinforced polymer composite

Fiber-reinforced polymer (FRP) composite filament is a widely used way of improving the FFF-printed parts' mechanical properties. First, polymer pellets are mixed with the reinforced fiber in a blinder; after that, mostly twin-screw extruder extrudes the mixture, then a second extrusion process for the filament materials for a better homogeneity if required.

Carbon and glass fibers are the most used fibers for FFF; they provide superior properties for the FRP composite printed parts such as corrosion and wear resistance, high strength-to-weight ratio and better dimensional stability. FFF-printed parts made of short carbon fiber-reinforced ABS enjoy elastic modulus and tensile strength 700% and 115% higher than those values of pure ABS parts at 40 wt.% carbon fiber loading (Tekinalp et al. 2014). Continuous carbon fiber also has been used as a reinforcing phase for the PLA matrix (Matsuzaki et al. 2016); results

showed 599% and 435% improvement in the elastic modulus and strength of the composite compared to the pure PLA FFF-printed parts. However, some discontinuity and irregularity of the carbon fibers were observed in the printed parts.

Although carbon and glass fibers reinforced polymers composite provide a superior mechanical property for FFF-printed parts, their huge impact on the environment is still a concern. Nowadays, there is a trend to develop natural fiber reinforced polymer composite for FFF using wood, bamboo, and vegetable fibers (Mohan et al. 2017).

1.3.2 Particle-reinforced polymer composite

Incorporating particles into the polymer matrix is another commonly used method to improve the FFF-printed parts' final properties. The composite filament fabrication process is the same method used for fiber-reinforced polymer composite filament mentioned above. Several particles have been used as a filler for FFF, like glass bead aluminium oxide and ceramic. Ceramics particles like hydroxyapatite were also added to the PLA matrix with superior properties as a filament for medical applications (Mohan et al. 2017; Wang et al. 2017). The addition of iron and copper to the ABS matrix has shown a great improvement in the composite FFF-printed parts' storage modulus (stiffness) compared to the pure ABS printed parts (Nikzad, Masood, and Sbarski 2011).

1.3.3 Nanocomposite

The unique and outstanding mechanical and thermal properties of nanofiber and nanoparticle make the addition of these nanoscale materials into the polymer matrix promising for the FFF to fabricate high functional parts for different applications. ABS-organic modified montmorillonite nanocomposite filament with filler loading of 5% has shown an outstanding tensile strength of the printed specimens with 43 % improvement than the pure ABS FFF-printed parts (Weng et al. 2016). Nanocomposite filaments for FFF are consuming more attention nowadays.

Researchers worldwide are looking to provide high strength nanocomposites filaments that can be used to fabricate functional parts for load-bearing applications.

In general, several parameters affect the polymer composite's final properties, including the shape, size, and distribution of the filler in the polymer matrix from one side and the interfacial adhesion between the filler and the matrix from the other side (Eirich 1978). The filler loading inside the polymer matrix is a critical issue that can significantly change the printed parts' mechanical properties. After a certain limit, the filler material starts to aggregate inside the polymer matrix, causing low strength properties (Bakır et al. 2021b). Furthermore, at high filler loading, filler material aggregates in the FFF machine's printing head, causing a nozzle clog that restrict the printing process. It was hard to make a continuous composite filament with carbon fiber loading more than 40 wt.% into the ABS matrix due to the loss of toughness (Tekinalp et al. 2014). Another critical issue is the formation of the voids around the filler. These voids are acting as a stress concentration inside the polymer matrix and deteriorate the final mechanical properties of the FFF-printed parts. One way of addressing the previous problem is by using surface-treated filler; surface treatment increases the compatibility between the two different phases resulting in excellent interfacial adhesion characteristics between the filler and the polymer matrix, thus better stress transfer properties.

CHAPTER 2

TUNABLE MECHANICAL PROPERTIES OF FOAMING PLA PRODUCED BY FFF

2.1 Abstract

Foaming polymers have drawn more attention in the last two decades in both the scientific and industrial communities. This new generation of polymers sheds new light on low density and multifunctional products used in several industrial applications, particularly for medical and energy absorption products. However, due to the high complexity of the foaming process, the applicability of these products depends mainly on their mechanical properties, which in turn have a high dependence on the processing parameters. FFF is one of the most AM technologies used to fabricate prototypes and products from different kinds of polymers. It provides an overall control on all the processing parameters to produce parts with desired characteristics. This study investigates the effect of the processing parameters, including (nozzle temperature, printing speed, flow rate, layer thickness, and infill ratio) on the mechanical properties of low-density polylactic acid (LW-PLA) produced parts by FFF. The results indicate that the nozzle temperature, flow rate, and infill ratio have the most significant effects on the printed parts' mechanical properties. Low nozzle temperature (230 °C), high flow rate (100 %) and high infill ratio (100 %) significantly improve the mechanical properties of the printed parts. On the other hand, layer thickness and printing speed have less significant effects than the other parameters; they should be in a good adjustment with the other parameters for better surface properties.

2.2 Introduction

Polylactic acid (PLA) is considered one of the most polymers used for FFF. The high biocompatibility and biodegradability of PLA make it a great candidate for medical and packaging products (Garlotta 2001; Lim et al. 2008). Moreover, the high biocompatibility and large surface area of PLA make the foaming form of PLA, achieved by dissolving a blowing agent in the polymer matrix, further applicable in the industry sector, especially for medical implant applications where the weight and the porosity of the printed parts are of great importance (Khodaei, Amini, and Valanezhad 2020; Li et al. 2019; Sanz-Horta et al. 2020). Low-density PLA (LW-PLA) is one kind that is working according to foaming technology (Colorfabb n.d.). Due to the high complexity of the foaming process, this new variation of PLA gets easily affected by changing the processing parameters, which requires a better understanding of the relation between the changing of the processing parameters and the mechanical properties of the printed parts.

One of the most precious advantages of FFF, particularly for the scientific approach, is the ability of FFF to produce parts with simple control, even at a local scale (Li and Sun 2008), on all processing parameters. Such ease in the processing control can give the manufacturer the chance to produce parts with the desired morphological, thermal, and mechanical properties. In the last two decades, a massive number of reported research have attempted to optimize the printing parameters of FFF for better-printed parts. Particularly the printing parameters that have a direct effect on the final properties of the printed parts such as nozzle temperature, layer thickness, flow rate, printing speed, and infill ratio (Bakır et al. 2021a; Chacón et al. 2017; Kaygusuz and Özerinç 2019; Torres et al. 2016; Uddin et al. 2017).

This study aims to investigate the effect of the printing parameters such as nozzle temperature, layer thickness, flow rate, printing speed, and infill ratio on the mechanical properties of LW-PLA 3D printed parts. Several mechanical testing techniques such as the tensile test, the compression test, and the shore hardness test have been performed. Furthermore, differential scanning calorimetry (DSC), thermal

gravimetric analysis (TGA), and scanning electron microscopy (SEM) have been performed for comprehensive analysis of the thermal, structural and mechanical behaviour of the printed parts.

2.3 Experimental Details

An open-source Ultimaker 2+ desktop 3D printer (Netherlands) based on FFF technology was used to print all the specimens. The input material filament LW-PLA, 2.85 mm in diameter, was purchased from Colorfabb, Netherlands, without providing details about the production process. However, this kind of filament usually achieved by first blowing an agent in the polymer matrix then followed by an extrusion process (Choi et al. 2020; Lim et al. 2008).

All the dog bone-shaped specimens used for the tensile test were based on American Society for Testing and Materials ASTM D 638 type 4 Figure 6 (a), one the other hand, cylindrical specimens 25.4 mm in both diameter and height, Figure 6 (b), have been used for the compression test. Furthermore, another rectangular specimen has been printed for shore hardness measurement Figure 6 (c). All specimens were printed with a raster orientation of $(-45^{\circ}, 45^{\circ})$ with respect to the axis of loading; zero top and bottom layer configuration was used for all specimens. All specimens also were printed with a line raster type, except for the specimens used for investigating the infill ratio effect was a grid raster type. Three identical specimens were considered for each set in the tensile and compression tests. Table 3 summarises the printing parameters that kept constant for the different tests in this study.

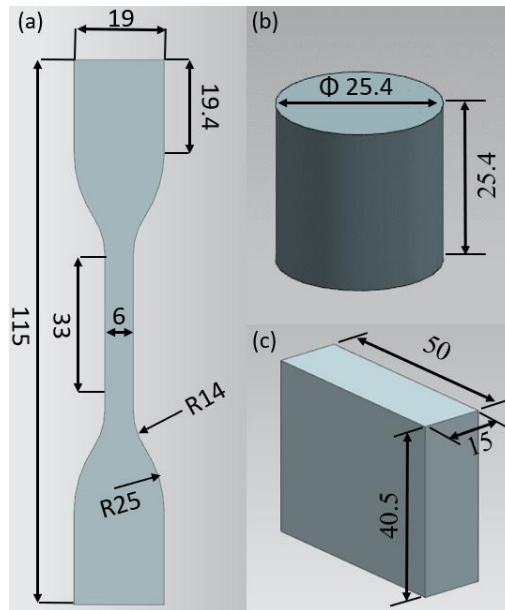


Figure 6. Schematic views of the specimen geometries. (a) Tensile specimen with a thickness of 3.2 mm, (b) compression specimen, (c) graded specimen for shore hardness measurements. All dimensions are in mm.

A Zwick/Roell (Z250), Germany, the universal testing machine, performed the tensile and compression tests. During the tests, the temperature has been kept at room temperature, and the displacement rate was 5 mm/min for both tensile and compression tests. For shore hardness measurement, a JIS type A hardness tester was used with a point of 0.79 mm diameter. The higher shore reading is for hard materials, and it goes down to lower values for soft materials.

Table 3. Printing parameters common to all specimens in LW-PLA study.

Filament diameter (mm)	2.85
Bed Temperature(°C)	60
Infill Pattern	±45
Inwall Layers	2 for specimens printed for infill ratio investigation, 3 elsewhere
Top and bottom layers	0

To get a clear insight on the effect of the printing parameters on the final properties of LW-PLA 3D printed parts, I investigated, in a systematic way, the effect of nozzle temperature, layer thickness, flow rate, printing speed, and infill ratio. Table 4 summarize the printing parameters investigated in this study with three identical specimens for a set of a parameter.

A TA instrument DSC 250 (USA) performed the differential scanning calorimetry (DSC) on the specimen and the filament. The samples were heated in the temperature range between 50-250 °C, and the filament was heated in the temperature range between 50-250 °C with a heating rate of 10 °C/min for all. The analysis was carried out under a nitrogen atmosphere to prevent degradation.

A Perkin Elmer Pyris 1 (USA) performed thermogravimetric analysis (TGA), the filament is heated in the range between 25-500 °C. The heating rate used was 10 °C/min in a nitrogen atmosphere to prevent degradation.

Scanning electron microscopy (SEM) was used in order to get insight into the fracture morphology. SEM was performed by A QUANTA 400F (FEI- Hillsboro-Oregon) field-emission SEM to analyze the fracture surfaces of the printed specimens at 20 kV. Before imaging, specimens were coated by 10 nm Au-Pd.

The shore hardness specimen was printed at a flow rate varying between (20-100) % in the z-direction, where the other parameters were nozzle temperature of 230 °C, the layer thickness of 0.45 mm, the printing speed of 45 mm/s, and the infill ratio of 100%.

Table 4. The printing parameters investigated in LW-PLA study.

Parameter	Range of Values Considered				Fixed Parameters						
					ND* (mm)	NT* (°C)	LT* (mm)	FR* (%)	PS* (mm/s)	IR* (%)	IT*
NT* (°C)	215	230	245	260	0.4	-	0.45	100	50	100	Line
LT* (mm)	0.2	0.35	0.5	0.7	0.6	230/245	-	100	50	100	Line
FR* (%)	100	75	50	25	0.4	230/245	0.45	-	50	100	Line
PS* (mm/s)	50	37.5	25	-	0.4	230/245	0.45	100	-	100	Line
IR* (%)	100	75	50	25	0.4	230	0.45	100	50	-	Grid

* ND: nozzle diameter, NT: nozzle temperature, LT: layer thickness, FR: flow rate, PS: printing speed, and IR and IT: infill ratio and type, respectively.

2.4 Results and Discussion

2.4.1 Effect of Nozzle Temperature

Four different nozzle temperatures are investigated in the range of 215 – 260°C. This range is slightly beyond what the manufacturer recommends (245 – 260°C) (Colorfabb n.d.). Figure 7 shows the stress-strain curves for each case. The results demonstrate the good repeatability of measurements and the large influence of nozzle temperature on the mechanical behaviour. The flow stress and the slope of the elastic response show a monotonic increase with decreasing temperature. The decrease in the elastic modulus of PLA FFF-printed specimens was also found in the literature review with a reduction of 20 % by increasing the nozzle temperature from 215 to 230 °C (Abeykoon et al. 2020). Elongation at break remains relatively constant and does not exhibit a clear trend with nozzle temperature.

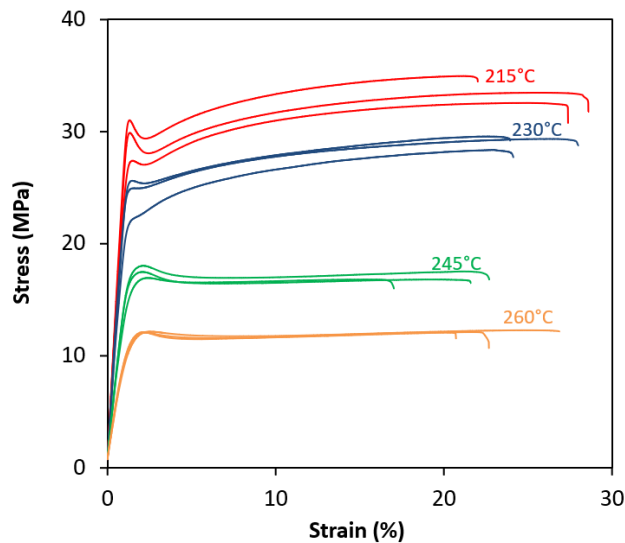


Figure 7. The stress-strain curves for specimens printed at different nozzle temperatures.

Figure 8 shows the average mechanical properties, density, and density-specific mechanical properties as a function of nozzle temperature. Both tensile strength and elastic modulus monotonically decrease with temperature. The nozzle temperature

of 215°C yields a tensile strength of 33.2 MPa and an elastic modulus of 2.6 GPa. When the nozzle temperature reaches 260°C, the strength and the modulus decrease almost by a factor of three, and becomes 12.1 MPa and 0.96 GPa, respectively.

Elongation at break has a slightly decreasing trend with increasing nozzle temperature. However, the variations are comparable to the standard deviation of the data. Therefore, there is no statistically significant effect of nozzle temperature on elongation at break. Density also monotonically decreases with increasing temperature but at a lower rate compared to that of strength and elastic modulus.

Overall, the results show an extreme variation in mechanical properties with nozzle temperature, which is a unique behaviour not observed in conventional filaments. Previous studies in the literature show that the nozzle temperature affects the strength through the level of fusion in between printed layers. The nozzle temperature directly affects the available thermal energy at the interface of the incoming line of polymer and the existing polymer, which directly translates to the quality and extent of fusion between printed lines and layers. When the nozzle temperature is low, poor fusion frequently results in lower strength and ductility. The nozzle temperature is also known to affect the crystallinity of the printed part. For example, an increase in the nozzle temperature increases the cooling rate and reduces the PLA crystallinity in PLA-PHA blend filaments. However, the findings so far in the literature suggest that this effect is mostly secondary compared to the level of fusion phenomenon (Kaygusuz and Özerinç 2019).

The foaming PLA's mechanical properties exhibit a stronger dependence on the nozzle temperature as the nozzle temperature directly influences the foaming characteristics. Figure 9 demonstrates this behaviour – as nozzle temperature increases, the gas bubble density increases. The rise in the extent of foaming is more pronounced, especially when the nozzle temperature increases from 230 to 245°C. The results are in agreement with the density measurements, which showed a monotonic decrease with nozzle temperature. The increase in the extent of foam reduced the solid volume fraction and the cross-sectional area fraction for load-

bearing caused a reduction in tensile strength and elastic modulus. Another important point is the fragile structure accompanied by the increase in the foam density in the polymer matrix since the last will lead to more fragile walls surrounding the foams, causing another reason for the poor strength properties. Furthermore, the microscope images of Figure 9 shows excellent fusion between the rasters even for the lowest nozzle temperature of 230°C. Therefore, I conclude that the variations in the mechanical properties are primarily caused by the foaming behaviour.

Figure 8 (d) shows the specific strength and specific modulus, which are strength and modulus values normalized by the respective density of the specimens. As the nozzle temperature increases and the density decreases, the specific strength and modulus decrease.

Two ways were used to measure the density; first, I cut a square piece of a specimen then measured the volume and the weight of that specimen to get its density. Second, I separately print only the gauge length, then measure the volume and weight, and get the density. In both approaches, the density of a specimen printed at the same printing parameters was the same.

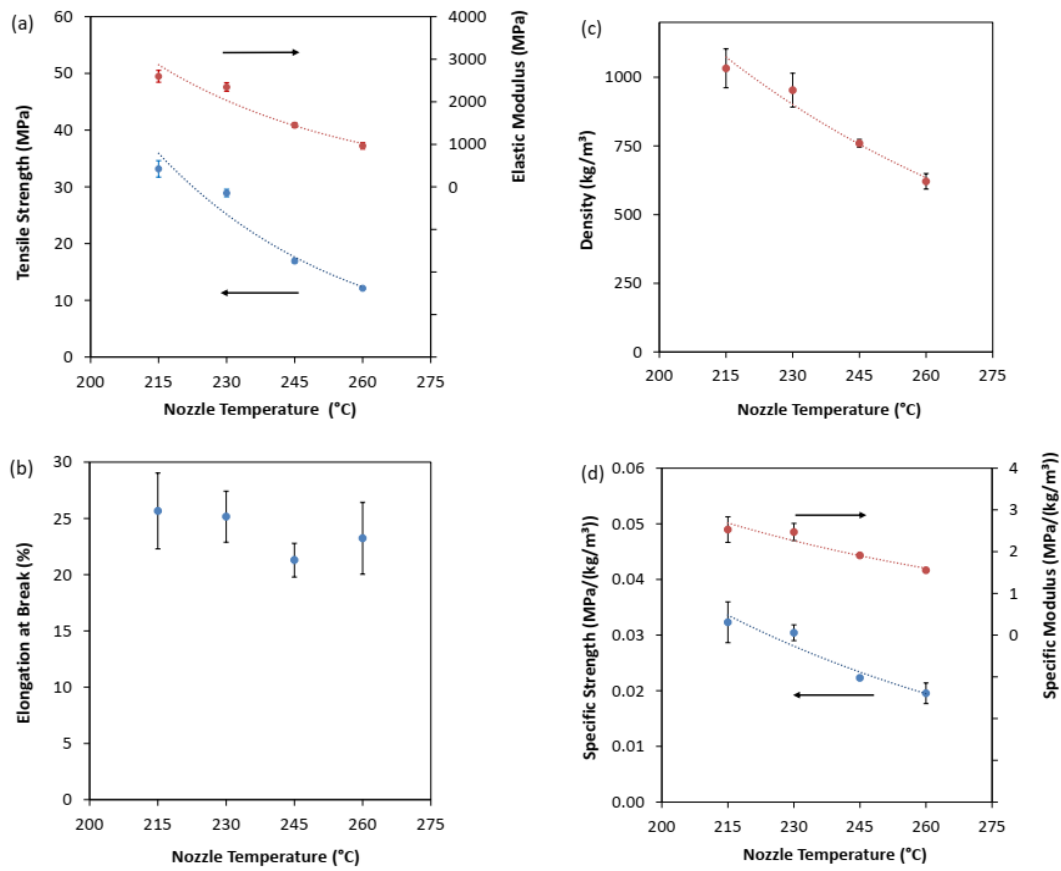


Figure 8. (a) The tensile strength and elastic modulus, (b) the elongation at break, (c) the density, and (d) the specific properties of the printed specimens at different nozzle temperatures. The error bar represents one standard deviation obtained from testing three samples. The error bar at 260 °C Figure (a) is very small to be shown.

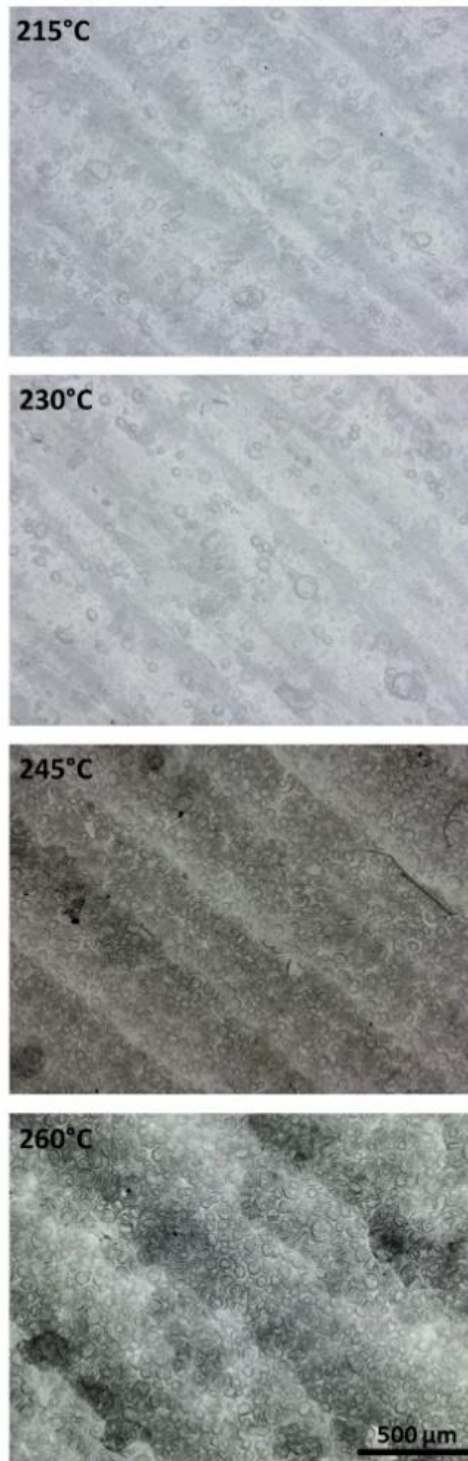


Figure 9. Optical microscope images of the printed specimens as a function of nozzle temperature.

2.4.2 Effect of Filament Flow Rate

Filament flow rate defines the rate at which the feeder mechanism of the printer feeds the filament into the printing head. Therefore, it is a parameter that ensures that the correct amount of filament is provided for the continuous printing of lines. Figure 10 shows the mechanical properties of specimens printed at four different flow rates (100, 75, 50, and 25 %) at two different nozzle temperatures (230 and 245°C). Both tensile and elastic modulus follow the same trend with a sharp decrease by decreasing the flow rate in both nozzle temperature sets. When the flow rate decreased from 100 to 25 %, both mechanical properties' values decreased by more than 60, and 80 % at 245, and 230 °C, respectively. To analyze the effect of this parameter more comprehensively, it is better first to understand the foaming process under different flow rates. For that reason, an SEM analysis was performed to analyze the fracture surfaces of specimens printed at different flow rates 100, 50, and 25 %, at nozzle temperature of 230 °C, Figure 11. It can be clearly seen that at a high flow rate of 100 %, there is more fusion between the successive layers leading to better strength and tensile resistance properties (Aliheidari et al. 2017; Valerga Puerta et al. 2019). Also, fewer foams have been detected. However, by decreasing the flow rate to 50 %, the interlayer adhesion becomes weaker, and it becomes even possible to see each individual layer Figure 11 (b). Furthermore, more and smaller foams have been detected on the fracture surface, leading to more thin walls inside the printed samples and eventually a faster failure at low loads. The effect of flow rate becomes more severe at 25 % Figure 11 (c); the foams start to emerge inside of each other, leading to the found low strength properties. Table 5 summarizes the foams characterization at different flow rates (%).

The elongation at break follows a different path; at 230 °C nozzle temperature, the elongation decreases sharply with decreasing the flow rate. However, at 245 °C, the elongation slightly increases as the flow rate decreases until 50 % flow rate, then it drops sharply at any further decrease in the flow rate. Furthermore, Figure 10 (c) shows that by decreasing the flow rate, the samples' density decreases since less

material will be used to print the samples at a low flow rate. Specific mechanical properties are also presented in Figure 10 (d), indicating that the flow rate decrease slightly decreases the specific properties at 230 °C. However, at 245 °C, the specific properties kept almost the same regardless of the decrease in the specimen's density with decreasing the flow rate.

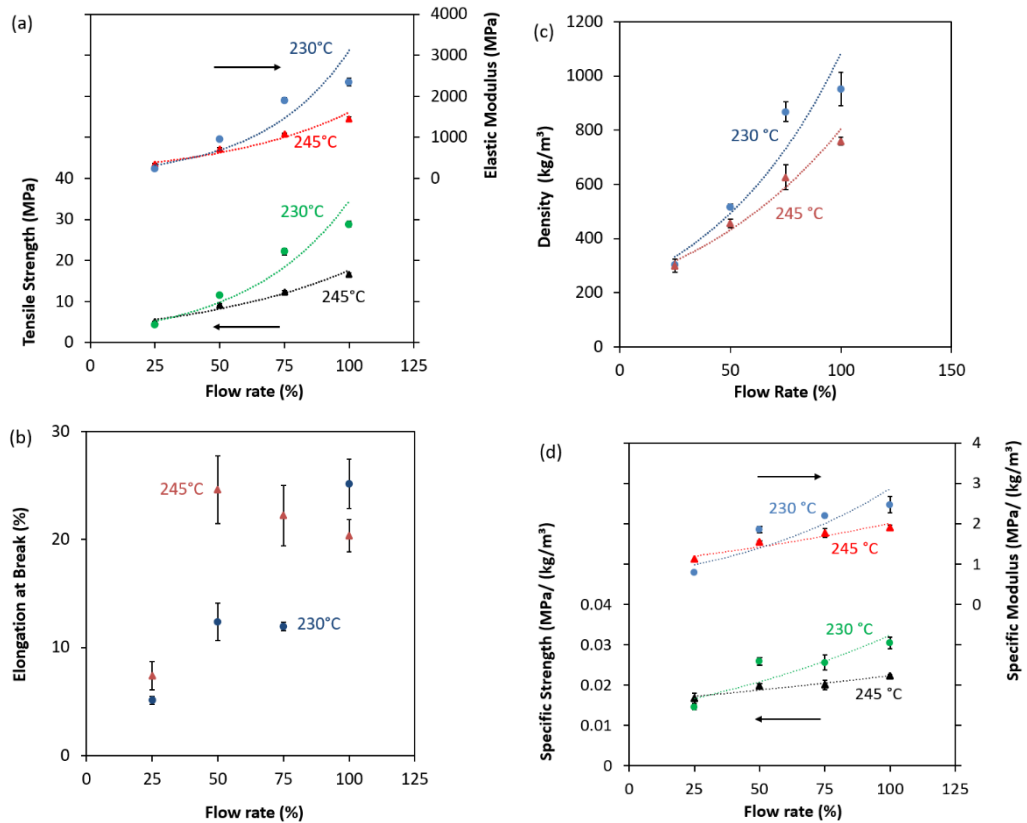


Figure 10. (a) The tensile strength and modulus, (b) the elongation at break, (c) the density, and (d) the specific tensile strength and modulus of the printed specimens at different flow rates at two nozzle temperatures at 230 and 245 °C.

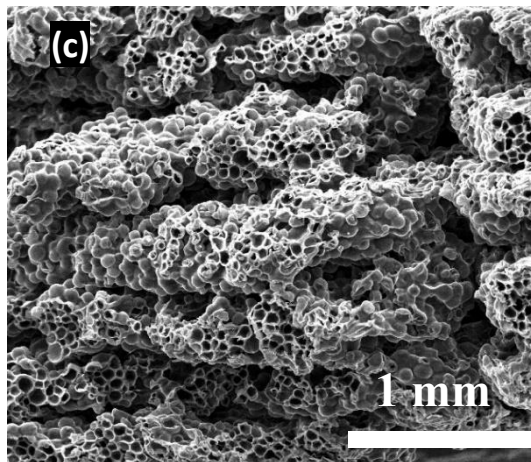
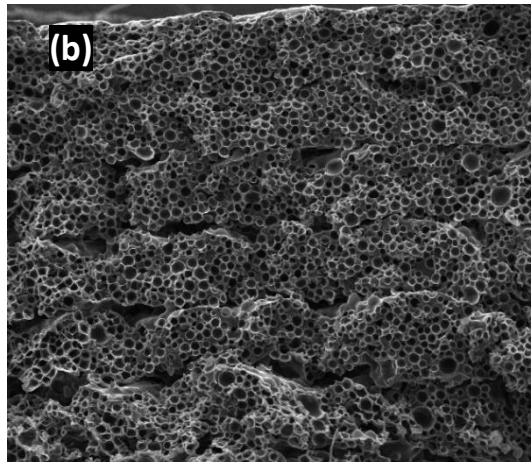
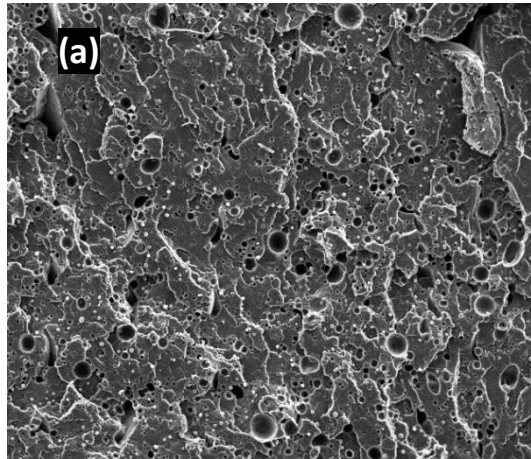


Figure 11. Cross-section SEM images of 3D-printed samples with a variable flow rate of (a) 100 %, (b) 50 %, (c) and 25 %.

Table 5. LW-PLA Foams characterization at different flow rate (%) based on SEM images of Figure 11.

Flow Rate (%)	100	50	25
Foam Area (μm^2)	219.04	777.01	1251.31
Foam Area (%)	23.82	56.62	83.35

Foam area is calculated by using ImageJ software. An SEM image is uploaded to this software which works according to contrast filtering; then, due to the variation in colour between the foams and the walls surrounding the foams, it becomes easy to calculate the area that the foams occupy. Usually, several SEM images for different spots of the same sample are used for more accurate calculations.

2.4.3 Effect of printing speed

Printing speed refers to the speed of the nozzle in any direction during printing. Figure 12 (a)-(d) describes the samples' mechanical properties, specific properties, and densities printed at different printing speeds at two sets of nozzle temperatures. Results indicated that, at a low nozzle temperature of 230 °C, the tensile strength and elastic modulus follow a fluctuation trend with slight improvement by 6 and 11 % at 37.5 mm/s then a decrease to their original values at 25 mm/s. However, the variations are comparable to the standard deviation of the data, so there is no significant effect on the printing speed on the strength properties at 230 °C. On the other hand, the elongation at break decreased slightly with the decrease in the printing speed; the printing speed has more effect on the surface properties than on the printed parts' mechanical properties (Anitha, Arunachalam, and Radhakrishnan 2001; Zhao et al. 2020).

The slight decrease in the strength properties at 245 °C nozzle temperature with decreasing the print speed can be attributed, to a great extent, to the effect of the nozzle temperature more than to the printing speed effect. At low speed, the polymer will be exposed more to the heat, which in turn leads to more foams inside the polymer melt and eventually weakens the printed parts. Furthermore, the elongation

at break has not been affected by the printing speed at this temperature. Moreover, Figure 12 (c) shows that the density values do not get affected by the printing speed at 230 °C. However, by increasing the nozzle temperature, the increase in the foam inside the polymer melt leads to a decrease in the density of the samples by decreasing the printing speed. Furthermore, Figure 12 (d) shows that the printing speed has a minor effect on the specific properties that can be neglected.

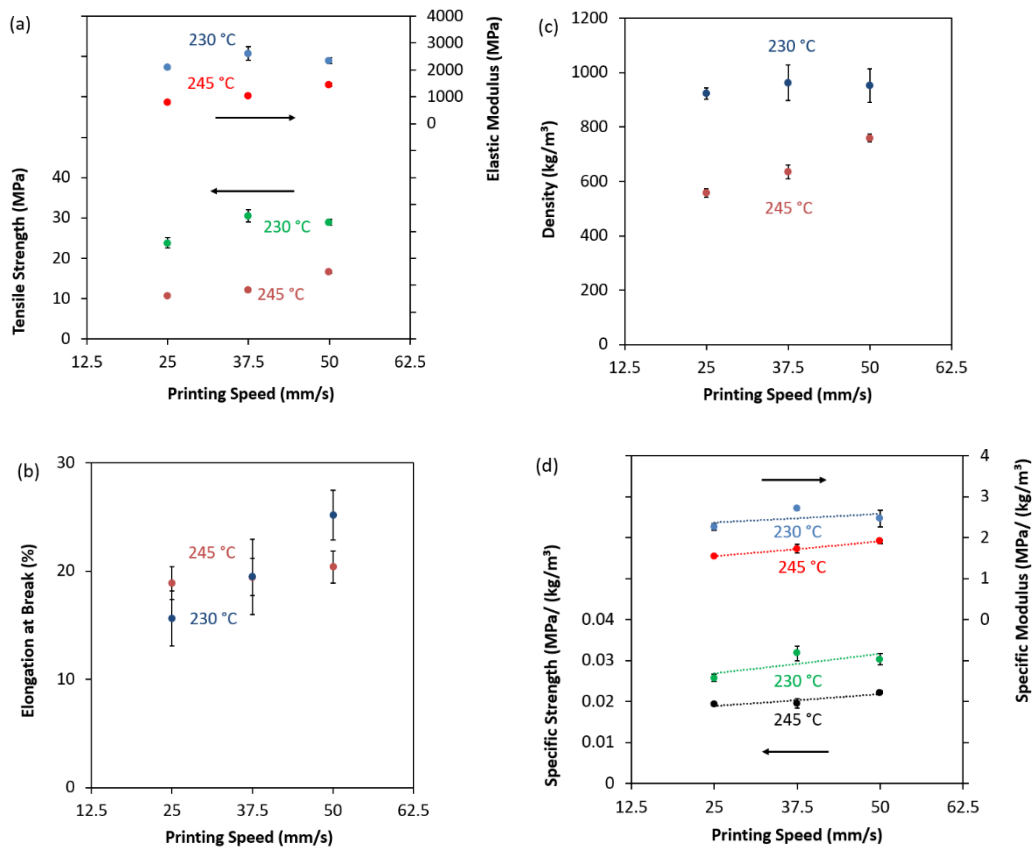


Figure 12. (a) The tensile strength and elastic modulus, (b) the elongation at break, (c) the density, and (d) the specific tensile strength and modulus of the printed specimens at different printing speeds at two sets of nozzle temperature.

2.4.4 Effect of infill Ratio

This parameter represents the distance between the adjacent rasters; several studies have considered a 70- 80 % infill ratio, resulting in good tensile properties and saving

more time and material (Samykanon et al. 2019; Zandi et al. 2020). Figure 13 (a)-(b) show the mechanical properties of samples printed at different infill ratios (%). Results show that as the infill ratio decreases, both tensile strength and elastic modulus decrease sharply with a reduction of 60 % for both values with decreasing the infill ratio from 100 to 25%. Previous studies in the literature show that by decreasing the infill ratio, the strength properties decrease sharply. The tensile strength and the elastic modulus of the FFF-printed recycled polyethylene terephthalate (rPET) filaments decrease by 21 and 17 % with decreasing the infill ratio from 100 to 80 % (Bakır et al. 2021a).

Elongation at break has a fluctuation trend with decreasing the infill ratio. However, the variations are comparable to the standard deviation of the data. Therefore, there is no statistically significant effect of infill ratio on elongation at break. Figure 13 (c) shows the densities that sharply decreased by decreasing the printed specimens' infill ratio. On the other hand, the specific properties kept almost at the same values at any infill ratio Figure 13 (d). Figure 13 (e) shows an image of tested specimens printed for the infill ratio investigation. Specimens printed at 25 % infill ratio experience a break out of the gauge length due to the high-stress concentration at that region, and the results should be approached with caution. In spite of this problem, the obtained results are in agreement with the general trends.

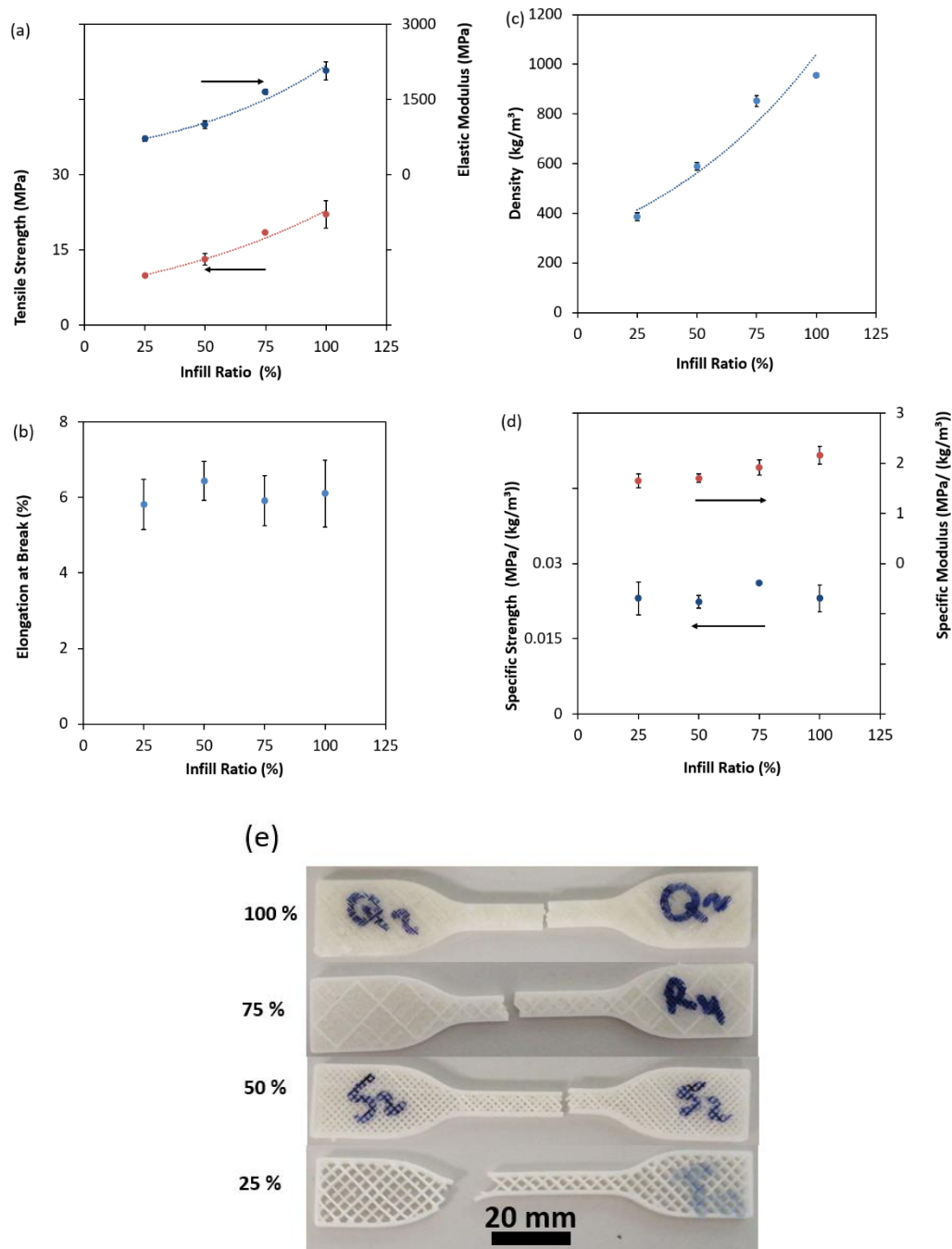


Figure 13. (a) The tensile strength and elastic modulus, (b) the elongation at break, (c) the density, (d) the specific properties, and (e) the image of the specimens printed specimens at different infill ratios.

2.4.5 Effect of Layer Thickness

The effect of layer thickness is investigated by printing specimens with four different sets of layer thickness (0.2, 0.35, 0.5, and 0.7 mm) at two different nozzle temperatures (230 and 245°C). Results show that the layer thickness has a relatively smaller effect on the mechanical properties than the other parameters. The results did not show any clear trends; therefore, I only provide some key values for this parameter. For the nozzle temperature of 230°C, 0.5 mm layer thickness yielded the highest tensile strength and elastic modulus, 33.3 MPa and 3.14 GPa, respectively. On the other hand, 0.35 mm layer thickness provided the largest elongation at break (30%). At the higher nozzle temperature of 245°C, 0.7 mm layer thickness yielded the best results with a tensile strength of 22.5 GPa and an elastic modulus of 2.08 GPa. For density, in both nozzle temperatures, the change in the layer thickness does not affect the density of the specimens, Figure 14.

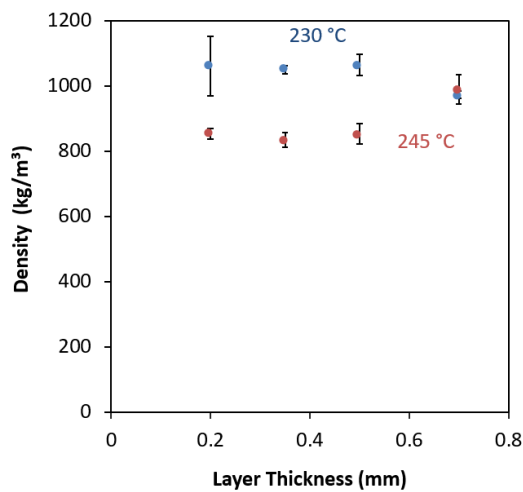


Figure 14. The densities of specimens printed at different layer thicknesses.

Figure 15 summarizes all specimens' tensile, modulus and specific strength as a function of their densities printed at different printing parameters and tested by the tensile testing machine. As the specimen density increases, the load-bearing capacity will increase since the thickness of the walls surrounding the foam will increase.

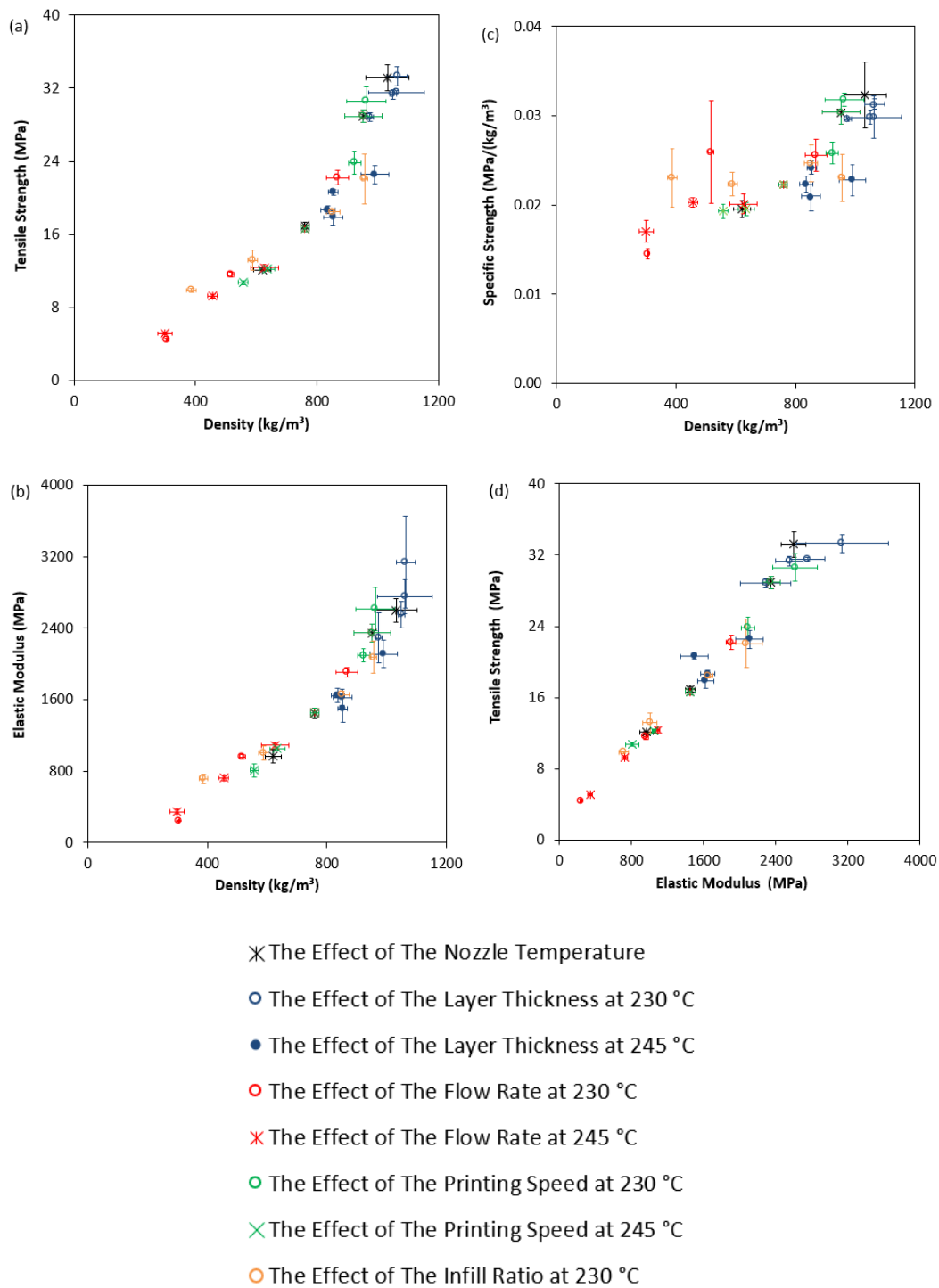


Figure 15. (a) The tensile strength - density, (b) the elastic modulus - density, (c) the specific strength - density, and (d) the specific strength - the elastic modulus figures of all specimens printed at different printing parameters.

By applying the knowledge and concept of Gibson-Ashby (GA) (1) of foamed materials, it becomes possible to drive a mathematical model that can predict a mechanical property at any foamability degree (Gibson and Ashby 1997).

$$\frac{E_F}{E_S} = \varphi^2 * \left(\frac{\rho_F}{\rho_S}\right)^2 + (1 - \varphi) * \left(\frac{\rho_F}{\rho_S}\right) \quad (1)$$

E is the elastic modulus, and subscript S and F refer to the fully solid and foamed specimens. The fitting constant φ represents the portion of the strut in the foamed material. Figure 16 (a) compares the experimental results and results I get by using (1). According to the AG model, the constant φ is equal to 0.85, which agrees with what was found in the literature review for polyurethane with 0.85 (Ramsteiner, Fell, and Forster 2001) and 0.8 (Calvert et al. 2010). On the other hand, the tensile strength also was found to fit the AG model with the same constant ($\varphi=0.85$) according to (2), Figure 16 (b), where σ is the tensile strength (Ramsteiner et al. 2001).

$$\frac{\sigma_F}{\sigma_S} = 0.4225 * \left(\frac{\rho_F}{\rho_S}\right)^{1.5} + (1 - \varphi) * \left(\frac{\rho_F}{\rho_S}\right) \quad (2)$$

All the mechanical properties for the solid calculation were taken from (Farah et al. 2016).

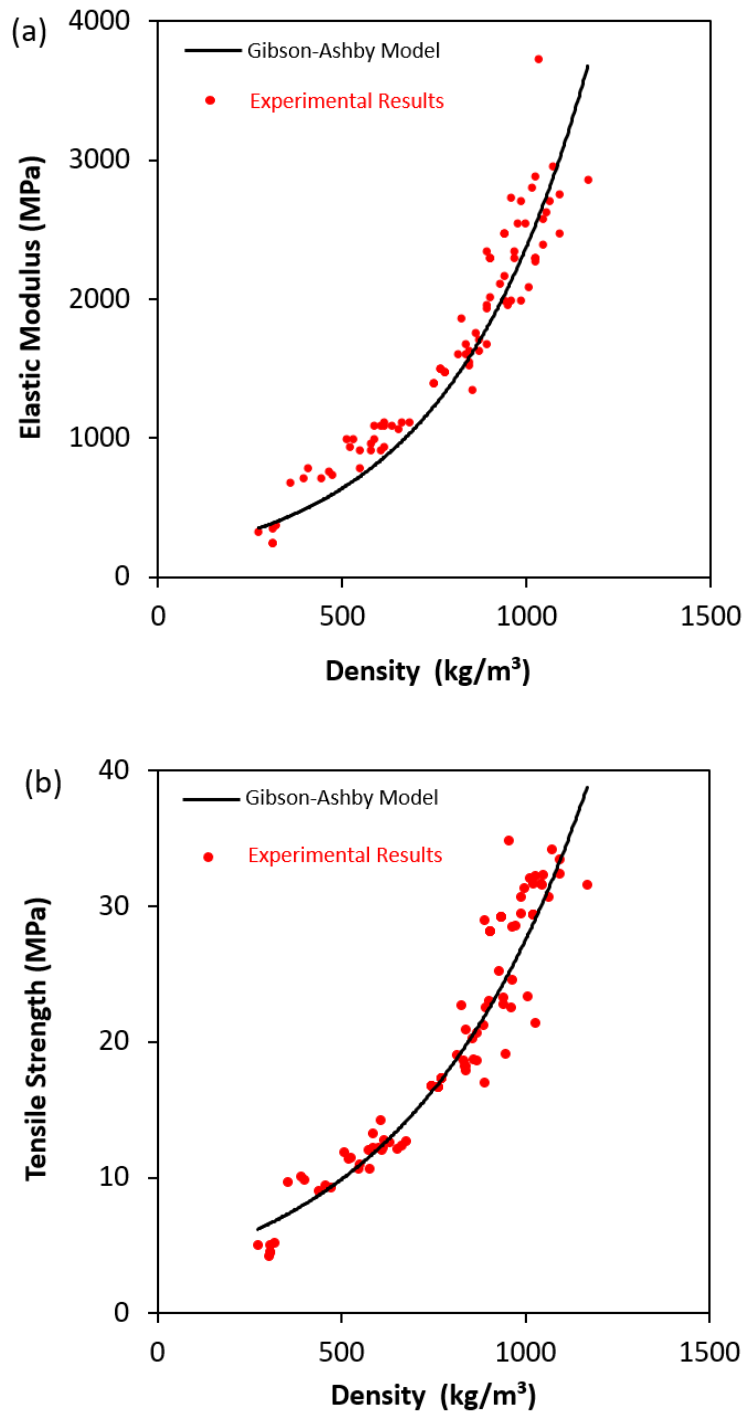


Figure 16. (a) The tensile strength - density, and (b) the elastic modulus - density figures of all specimens printed at different printing parameters calculated experimentally and theoretically according to Gibson-Ashby model.

2.4.6 Compression test

I only investigated the flow rate effect on the compressive properties for the compression test, namely, maximum compressive strength and compressive modulus. Figure 17 represents the compressive mechanical properties and specimens' densities printed at different flow rates of 100, 75, 50, and 25 (%) at 230 °C nozzle temperature. Results indicate that the compressive strength and modulus decrease sharply by decreasing the flow rate, a reduction of 95% in both properties was observed by decreasing the flow rate from 100 to 25 %. A low flow rate means producing more and smaller foams leading to more thin walls inside the printed part and eventually reducing the strength properties; it was also found in the literature that high porosity deteriorates the compressive strength of the 3D printed parts (Singh et al. 2019). When it comes to the density and the specific properties, decreasing the flow rate is accompanied by decreasing the printed specimens' density and specific properties. Compressed specimens printed at different flow rates are provided in Figure 18.

Energy absorption is one of the most applicable field for foaming polymers; the ability of the foaming structures to absorb energy and mitigate shock loadings relies on its compression response. Experiencing compressive stress, polymer foams undergo a linear-elastic deformation with stretching or/and bending of the cell walls. At higher stress, these walls dissipating energy when they collapse and buckles. For the closed-cell foam structure, the compression of the air trapped inside the closed foams forms a significant additional contribution to the energy absorption characteristic of the closed-foam structure (Bishop and Smallman 2002); in other words, the foaming density greatly affects the energy absorption behaviour of the structure. Therefore, by considering the ability to tune the foam density of the LW-PLA FFF-printed parts, one promising application is by fabricating a density-tuned printed part with higher foam density where more energy dissipation is required.

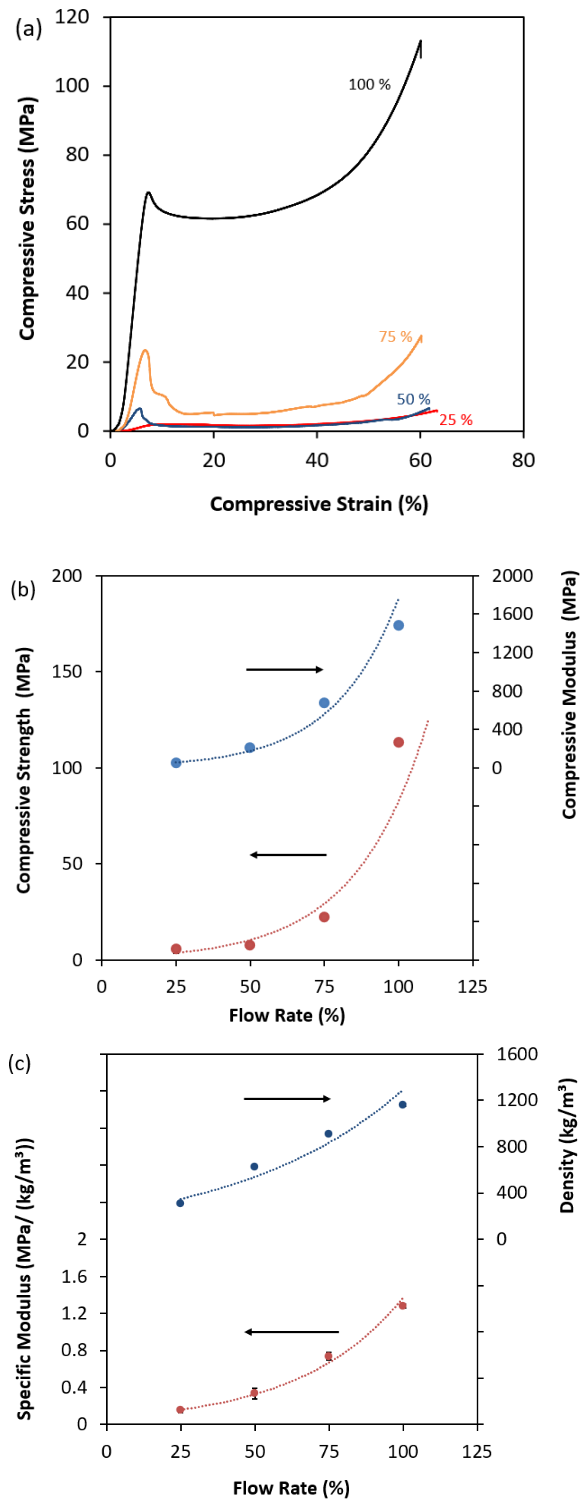


Figure 17. (a) The compressive stress-strain curves, (b) the compressive strength and modulus, and (c) the specific modulus and densities.

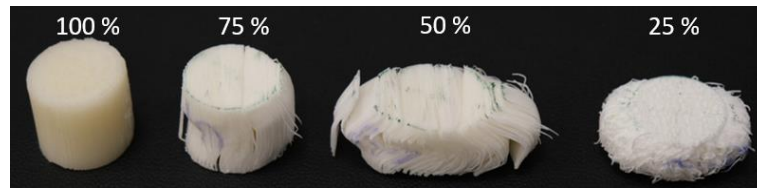


Figure 18. The image of compression specimens printed at different flow rates (%).

2.4.7 Shore hardness measurement

Shore hardness represents the resistance of a material to indentation. This study investigated the shore hardness of a block with 50 mm ×15 mm×40.5 mm dimensions by fabricating this block with decreasing flow rate as the printer's platform goes down in the z-direction. By reducing the flow rate, the surface quality decreases with the appearance of more gaps on the surface that can affect the reliability of the measurement; for that reason, I took five measurements at different points for each flow rate set. Figure 19 shows the average shore hardness at a different flow rate. Results indicate the increase in the softness as the flow rate decreases with the softest part of 54.7 shore A at a 20 % flow rate. Specimens with a higher flow rate enjoy denser interlayer structure with smaller gap size between the successive layers, therefore more resistance for indentation.

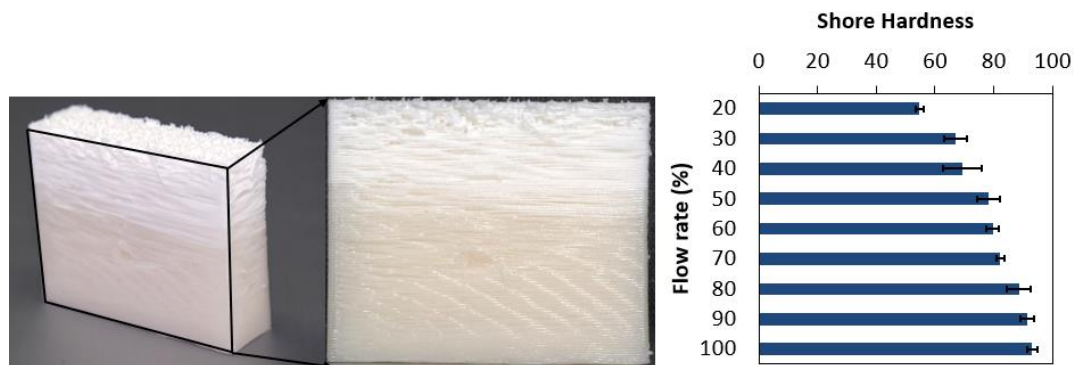


Figure 19. The shore hardness at a different flow rate. The error bar represents one standard deviation obtained from measuring five different points.

2.4.8 Thermal characterization.

2.4.8.1 Differential scanning calorimetry (DSC).

Figure 20 (a) shows the DSC of the filament and specimens printed at different nozzle temperatures. The first heat curve will be considered since it provides a more accurate thermal history of the polymer investigated.

Table 6 shows the results of DSC the glass transition temperature (T_g), crystallization enthalpy (ΔH_{cc}) and melting enthalpy (ΔH_m) of the filament and the specimens printed at different temperatures. The degree of crystallization (%X) is calculated by (3), where (ΔH_{m0}) is the melting enthalpy at 100 % crystallinity which equals 93 Jg^{-1} (Branciforti et al. 2009; Moura et al. 2019). The low degree of crystallinity of the filament asserts the mostly amorphous behaviour of the PLA filament. However, this value is very low compared to the literature review (22 %) (Kaygusuz and Özerinç 2019). On the other hand, the increase in the nozzle temperature reduces more the degree of the crystallinity by increasing the cooling rate, which also found in the PLA crystallinity in PLA-PHA blend filaments. Although the DSC's values cannot give an absolute result of the degree of the crystallinity, it gives an overview of the effect of the nozzle temperature on the amorphous behaviour of the specimen (Kaygusuz and Özerinç 2019). One way to improve the low crystallinity of PLA is by applying post-processing annealing at a temperature above the glass transition temperature and below the melting temperature (Wach, Wolszczak, and Adamus-Wlodarczyk 2018). Overall, introducing the blowing agent for foamability deteriorates the crystallinity degree of the polymer. However, it does not affect the glass transition temperature since the last keeps its value in the range 50-70 °C found in the literature review of neat PLA (Basu et al. 2017; Zilberman 2005).

$$\%X = \frac{\Delta H_m - \Delta H_{cc}}{\Delta H_{m0}} \quad (3)$$

Table 6. DSC test results of LW-PLA.

	T_g (°C)	ΔH_{cc} Jg⁻¹	ΔH_m Jg⁻¹	%X
Filament	59.71	22.49	27.35	5.23
Specimen at 215 °C	60.99	18.99	23.17	4.50
Specimen at 230 °C	60.23	20.72	21.88	1.25
Specimen at 260 °C	58.51	22.84	20.08	—

T_g: The glass transition temperature, ΔH_{cc}: crystallization enthalpy, ΔH_m : melting enthalpy, and %X: the degree of crystallization.

2.4.8.2 Thermal gravimetric analysis (TGA)

Figure 20 (b) shows the TGA analysis of LW-PLA. TGA characterizes material by measuring the mass changing according to the change in the temperature. TGA usually be used together with DSC to provide a comprehensive interpretation of a material's thermal behaviour. The filament was heated to 500 °C under nitrogen condition. In this range of temperature, the polymer's pyrolysis happened at 375 °C with a loss of 94.4 % of the weight. This weight loss followed by another reduction in weight at 440 °C with a total weight loss of 98.29 %. On the other hand, derivative thermal gravimetric (DTG) is used to set the limits of the overlapping effects of decomposition and evaporation. The inflection point, also known as the first derivative peak temperature, is 383.11 °C which indicates the temperature at which the maximum rate of weight loss change occurred.

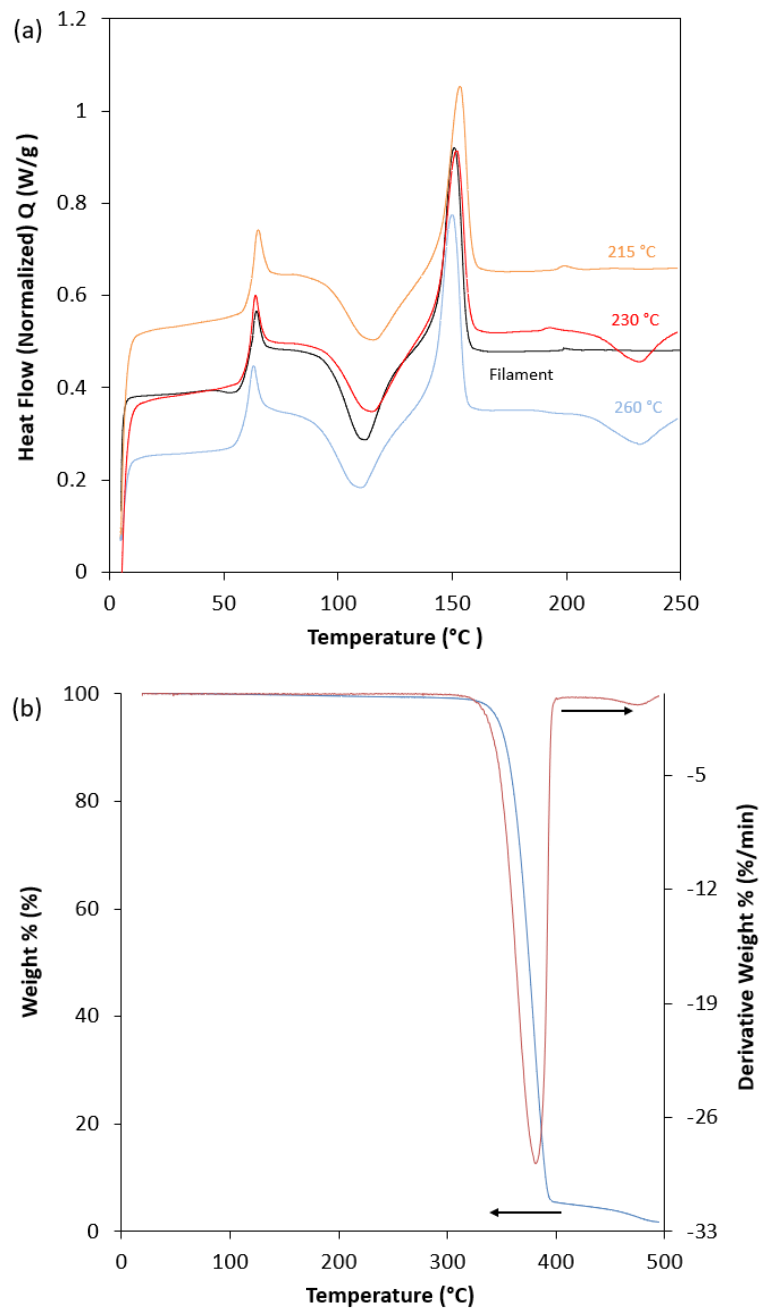


Figure 20. (a) The DSC of the filament and specimens printed at different nozzle temperature, heat flow endo up, and (b) the TGA of the filament used.

CHAPTER 3

DEVELOPMENT OF ABS-FLY ASH COMPOSITE FILAMENTS FOR FFF

3.1 Abstract

FFF is one of the most widely used additive manufacturing techniques for the fabrication of polymeric parts. Earlier applications of FFF mostly utilized pure polymers such as PLA and ABS. However, there has recently been an increasing demand for composite FFF filaments to obtain superior mechanical and physical properties. Fly ash (FA), a waste of coal power plants, is a promising alternative as a filler material for developing composite filaments. Due to the massive amounts of FA generated worldwide and associated environmental concerns, there has been an increasing trend in the utilization of FA particles in the polymer industry, providing a new route for FA recycling towards reducing FA's impact on the environment. However, there has been no study to date to investigate the same route for FFF use. In this study, I incorporated 2 wt.% FA into an ABS matrix using a twin-screw extruder and produced composite filaments for FFF. The specimens printed with the composite filament were tested for their microstructural, mechanical, and thermal properties through X-ray diffraction, tensile testing, differential scanning calorimetry (DSC), and thermogravimetric analysis (TGA). Overall, the properties of the composite specimens are not drastically different from those made of pure ABS, except for the decrease in the elongation at break. The results demonstrate the feasibility of using ABS-FA composites in FFF as a coloring agent that contributes to the recycling of waste material at the same time.

3.2 Introduction

The use of organic polymers in both the scientific and industrial sectors has been dominant in the past few decades. To obtain further improvement in their functionality and widen their application scope, the utilization of a second phase has been addressed efficiently to prepare composite polymers (Sun et al. 2013). Usually, it is possible to add one or more filler to the polymer matrix in order to enhance a certain mechanical, physical, or thermal property to produce lightweight, corrosion resistance, elevated temperature applicability, high strength, and cost-effective products. Generally, several parameters affect a polymer composite's final properties, including the shape, size, and distribution of the filler in the matrix of the polymer from one side and the interfacial adhesion between the filler and the matrix from the other side (Eirich 1978). Most powdered materials, with a low aspect ratio and low cost, can be used as fillers. However, the tendency towards natural-deposited fillers is gaining more attention. Of those kinds of fillers, the most widely used are calcium carbonate, mica, quartz, talc, silica flour, and different kind of clays (Guhanathan and Devi 2004). In recent years, the utilization of the FA as an inorganic filler in the polymer composite has attracted more attention.

3.1 FA

FA is one of the byproducts of pulverized coal-fired power stations used to generate electrical power. In general, coal consists of two parts combustible organic and inorganic mineral matters; during the pulverized coal's burning, under high temperature, in the boiler of the coal-fired power stations, only the combustible materials are burned out. On the other hand, the non-combustible mineral part of the coal, which occupies 10–50 wt.%, is converted to coal ash. The heavier part of the coal ash, the bottom ash, falls to the bottom of the boiler and to be collected there. The lighter part of the coal ash, 75-85 % of the total coal ash, that keeps suspended in the flue gas is carried off to a cooler zone, then cooling and solidification processes will occur to produce amorphous glassy ash particles before releasing the flue gas

into the atmosphere. After that, these ash particles will be collected as fly ashes by using several separation techniques, including electrostatic precipitators (up to 99.9 % efficiency), fabric filters, baghouses, or cyclones (Chou 2012). Figure 21 represents the FA production and collection in a pulverized coal-fired power plant.

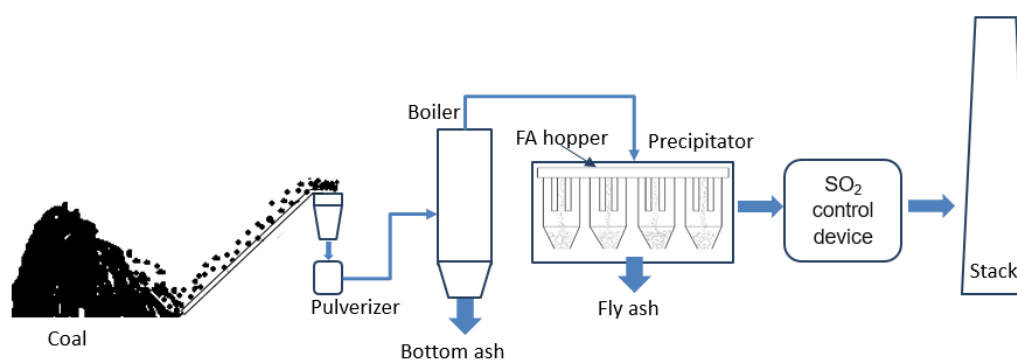


Figure 21. FA generation and collection in a pulverized coal-fired power plant (Adapted from (Chou 2012)).

The continuous increase in demand for energy worldwide has led to an increase in the reliance on coal-fired power stations leading to an increase in the FA produced all over the world. Although the FA world wide's high production, more than 700 million tons (MT) annually, FA's utilization is still a major concern, especially from an environmental perspective. Only 25 % of the produced FA particles are utilized in cement factories, structural fills, and mining applications. To get rid of the unutilized quantity of FA, people tend to dump FA on open lands or oceans. Such an inappropriate way of disposal leads to a catastrophic consequence on the environment and human health. FA particles are very small and can easily be suspended in the air, causing air pollution and posing some threats to human health who are repeatedly exposed to FA; here are some hazards of FA (Blissett and Rowson 2012; Dwivedi and Jain 2014; Joshi 1997; Yao et al. 2014).

- FA is considered a source of sand, air, and water pollution, with some heavy materials presented in the FA like Ni, Sb, Cd, Cr, As, Pb, etc.

- The fine FA particles can reach the lungs and accumulate there, causing some respiratory health problems. More even the FA submicron particles can go deeper into the lungs, raising the possibility of transferring the heavy metal to the blood plasma through the cells' membrane.
- FA has negative effects on the communities near the thermal power plants (TPP); suspended FA in the air can cause some reduction in the farms' agricultural productivity.

Therefore, FA recycling is considered the best available alternative to many environmental and economic benefits. Worldwide, four countries are responsible for most of the production of FA, namely India, China, the USA, and Germany. Figure 22 represents the FA production (million tons/year) and utilization (million tons/year) in different countries (Gollakota, Volli, and Shu 2019).

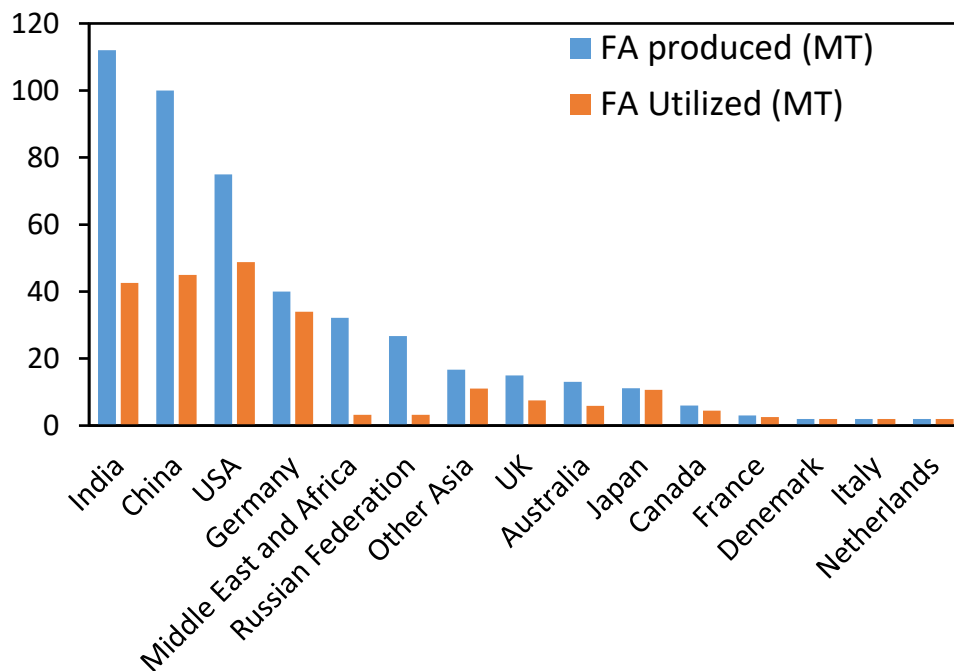


Figure 22. FA production and utilization (million tones (MT) /year) in different countries.

3.1.1 Classification of FA

According to ASTM C618, there are two types of FA based on the coal's origin.

- Type F: This type of FA is the byproduct of burning bituminous or anthracite coal; this type of FA enjoys pozzolanic characteristics.
- Type C: This type of FA is the byproduct of burning sub-bituminous or lignite coal. Along with the pozzolanic characteristics, type C FA also enjoys some cementitious properties.

Another important classification is based on the density and the size of the FA particles.

- Cenosphere-hollow particles, less than 1 g/cm^3 in density, can be used to prepare ultralight composites.
- Precipitator-spherical particles with a density between $2\text{--}2.5 \text{ g/cm}^3$ usually used to improve the FA-polymer composite's mechanical properties, including stiffness, wear resistance, and strength.

Some other sorts of FA classification are based on carbon content, SiO_2 solubility, SiO_2 reactivity, pozzolanic activity, etc. (K. Wesche 1991; Matsunaga et al. 2002; Satheesh Raja, Manisekar, and Manikandan 2014).

3.2 Characterization of FA

3.2.1.1 The physical properties of FA

In general, FA consists of fine amorphous particles that have a spherical shape, either hollow (cenosphere) or solid (precipitator). The main parameters that affect the shape and size of the FA particles are the uniformity and the source of the coal, the combustion uniformity, the pulverization degree, the level of the temperature and oxygen during combustion, and the collection system used to gather the FA particles

in the boiler. Furthermore, FA enjoys a porous hydrophilic surface, and the smaller the FA particles are, the more reactive, since

- Smaller FA particles enjoy larger specific areas, in other words, better bonding between the FA and the material matrix in the case of FA composite, and
- The rapid cooling of small FA particles results in more disordered particles, in other words, a more reactive structure.

Some physical properties are described in Table 7 (Ahmaruzzaman 2010; Anon 2002; Iyer and Scott 2001; Satheesh Raja et al. 2014).

Table 7. General physical properties of FA.

Fineness	(1 μm – 1 mm)
Specific gravity	(2.1 -3)
Specific surface area	(170 – 1000) m^2/kg
Colour	Gray*
Density	(Less than 1 – 2.5) g/cm^3
Particle shape	Regular, Irregular

* The FA colour may vary from grey to black according to the amount of unburned carbon is available.

3.2.1.2 The chemical properties of FA

In general, FA contains

- Some crystalline components like quartz, hematite, and mullite, and
- Some glassy components like silica glass and some oxides.

The main factors that affect the chemical and mineralogical component of FA particles are the origin and the type of coal used. On the other hand, some other

factors have some minor effects, such as the techniques used for handling, burning, or storing (Akin, Magalhães, and Kazanç 2020). FA consists mainly of

- Silicon dioxide (SiO_2), the principal sources of the SiO_2 in the FA are the clay minerals, and the quartz exists in the coal.
- Aluminium oxide (Al_2O_3), the principal sources of this content is the coal's clay and organic compounds.
- Iron oxide (Fe_2O_3), the existence of iron-containing materials in the coal is the main source of iron oxide.

Also, small concentrations of some alkali and metallic oxides may present. Table 8 describes the chemical composition of different types of FA (Ahmaruzzaman 2010; Anon 2002).

Table 8. The chemical composition of different types of FA.

Component (wt.%)	Bituminous	Sub- bituminous	Lignite
SiO_2	20–60	40–60	15–45
Al_2O_3	5–35	20–30	10–25
Fe_2O_3	10–40	4–10	4–15
CaO	1–12	5–30	15–40
MgO	0–5	1–6	3–10
SO_3	0–4	0–2	0–10
Na_2O	0–4	0–2	0–6
K_2O	0–3	0–4	0–4
LOI	0–15	0–3	0–5

3.2.2 FA in the polymer industry

In recent years, the utilization of the FA as an inorganic filler in the polymer composite has attracted more attention. FA causes some environmental problems and has no direct use except for a small volume of a fraction used in cement factories, structural fills, and mining applications (ACAA n.d.). However, FA becomes a very attractive filler for the plastic industry in recent years due to its low cost. Incorporating the FA in the polymer matrix will consume a volume fraction of the produced FA and improve some of the composite's final properties.

Several polymers have been used as a matrix for the polymer-FA composite, including PLA, ABS, High-density Polyethylene (HDPE), Polypropylene (PP), Epoxy Resin (ER), E-Glass Fiber Reinforced Polymer (GFRP), and others. These composites were fabricated by different manufacturing techniques like compression molding, casting, and injection molding. The FA size was between 5- 300 μm with loading of 5-60 wt.%. In order to get the desired size and content of the FA particles, several filtration techniques were used, namely grading techniques such as a series of cyclones, magnetic separator to separate magnetic particles, froth floatation to remove unburned carbon particles, high-energy planetary ball mill for nanoparticles, and standard mesh sieves.

The addition of 5 μm sized FA particles to PLA at 20 wt.% improved the tensile and impact strength of compression-moulded specimens by 80% and 40%, respectively. When the FA is surface treated (S-FA), these enhancements rise to 160% and 140%, respectively. Such improvement in the mechanical properties is due to S-FA particles' better surface properties leading to better bounding properties between the FA particles and the polymer matrix, thus improving the composite's strength properties. Any further increment of the FA/S-FA loading more than 20 wt.% leads to aggregation of the filler particles in the matrix and deteriorates the composite's strength properties (Xue, Bao, and Zhang 2016). Injection-moulded HDPE-FA composite specimens with FA loading (10-40 wt.%) show similar strength properties as those of the pure HDPE. However, the utilization of S-FA with the compatibilizer

agent's addition improve the tensile strength and elastic modulus by a factor of 1.4 and 1.6 at 20 wt.% and 10 wt.% FA and compatibilizer loading (Deepthi et al. 2010). The previous improvement in the HDPE-FA composite's elastic modulus was in good agreement with what was found in the literature review, 140 and 170 % improvement in the elastic modulus by the utilization of 30 wt.% FA and S-FA, respectively, into the recycled HDPE (r-HDPE) matrix. However, a sharp decrease in the tensile strength due to the crack propagation found around the FA/S-FA particles (Atikler, Basalp, and Tihminlioğlu 2006). One promising way of FA's utilization in the polymer industry is by the incorporation of FA into the PP matrix. S-FA reinforced PP composite, fabricated by compression molding, shows a great improvement in the elastic modulus by a factor of 3.7 at 60 wt.% S-FA loading with a small sacrifice in the tensile strength, reduction of 15 %. Such a high S-FA loading used in the composite with comparable results can make PP a good choice for polymer-FA composite with high FA's utilization (Pardo et al. 2010). Moreover, flexural strength and modulus also get some improvement by the addition of FA particles into the Polyester thermoplastic elastomer (TPE) matrix; both mechanical properties show 155 and 300 % improvement with the increase of the FA loading in the composite to 40 wt.% with better performance for smaller FA particles (Sreekanth et al. 2009).

When it comes to the elongation at break, all studies in the literature review show a drastic decrease with the addition of FA. This drastic decrease in the elongation values becomes more severe with increasing the FA loading with bad interfacial adhesion between the composite constitutes. FA particles interfere in the chain mobility of the polymer matrix, causing a very brittle composite, Table 9 represents a summary of some of the polymer-FA composites studied so far.

Table 9. Polymer-FA composites.

Polymer matrix	FA Size (μm)	FA Loading (wt.%)	Key results
ABS	9	10-50	Elastic modulus increases by 30 % at 30 wt.% FA. However, there was a reduction of 17 % in the tensile strength value of the composite at the same FA loading (Bonda, Mohanty, and Nayak 2012).
PLA	5	10-50	Tensile strength increases by 80 % at 20 wt.% FA, further improvement was also observed by 160 % by using surface modified FA particles. Impact strength follows the same trend with better performance at 20 wt.% FA with improvement of 45 and 140 % for the normal and surface modified FA particles respectively (Xue et al. 2016).
HDPE	106	10-40	Tensile strength increases by 40 % at 20 wt.% surface modified FA and by using 10 % compatibilizer agent (HDPE-g-dibutyl maleate). Elastic modulus increases by 60 % at 20 wt.% surface modified FA and by using 5 % compatibilizer agent. Elongation at break decreases drastically as the FA particles don't undergo elongation (Deepthi et al. 2010).
PP	110	0-60	Great improvement in the elastic modulus by a factor of 3.7 at 60 wt.% surface modified FA loading with a small sacrifice in the tensile strength of 15 % (Pardo et al. 2010).

3.2.2.1 Acrylonitrile-butadiene-styrene (ABS)-FA composite

ABS is an amorphous thermoplastic polymer that can be used widely in 3D printing technologies since it has a low T_g temperature, 105 °C. ABS enjoys excellent properties like (Dromel and Singh 2021; de Oliveira et al. 2018; Olivera et al. 2016; Omnexus n.d.; Wu and Li 2014);

- High toughness and rigidity,
- High dimensional stability,
- Good impact resistance, and
- Easy processing properties.

However, there are some drawbacks that hinder its usage like

- Inherent flammability,
- Low mechanical strength,
- Very sensitive to environmental conditions, and
- Poor weathering resistance properties.

The most important mechanical properties of the bulk ABS are listed below, Table 10 (Wypych 2016).

Table 10. The mechanical properties of ABS.

Elongation at Break	8 – 20%
Yield Strength	35 – 58 MPa
Elastic Modulus	1.9 – 2.7 GPa
Tensile Strength	25 – 65 MPa

In the past few decades, several researchers have focused on the ABS-FA composite to overcome some of the drawbacks of ABS from one side and to get rid of some volume fraction of produced FA. The addition of FA particles into the ABS matrix improves ABS's low thermal stability due to the FA's high degradation temperature

compared to the pure ABS. It also improves the composite's dynamic stiffness at a high working temperature (Bonda et al. 2012; Bonda, Mohanty, and Nayak 2016). On the other hand, the incorporation of FA particles into the ABS matrix has improved the mechanical performance, excluding the elongation at break, of the ABS-FA composite. The elastic modulus of ABS-FA composite with 30 wt.% FA/S-FA loading, fabricated by compression molding, was 1.3 times more than its value of the pure ABS specimens with a reduction of 17 % in the tensile strength values (Bonda et al. 2012). Another study also reported the reduction of the tensile strength by adding FA particles into the ABS matrix (Ramlan and Shuaib 2018); the main reason for that reduction was the insufficient stress transfer between the matrix and the filler due to the bad interfacial adhesion between them.

While preparing ABS-FA composite, there are some considerations for better mechanical performance (Bonda et al. 2012, 2016; Matsunaga et al. 2002; Ramlan and Shuaib 2018; Yang et al. 2006);

- FA particle size: small particles size improves the mechanical properties of the composite. FA particles with large sizes usually create small gaps inside the composite; those small gaps work as a stress concentration leading to a premature failure. Another important point For precipitator FA particles, as the size of the FA particles increases, the porosity will increase, reducing the elastic modulus of the FA particles.
- FA loading: the improvement of the mechanical properties enhances with the increase in the FA loading to a certain limit; beyond that limit, the mechanical properties start to deteriorate due to the agglomeration of the FA particles that weaken the composite.
- Surface modification of FA: S-FA particles have three times surface area more than the unmodified ones (Yang et al. 2006); also, the surface modification of the FA particles improves the adhesion between the FA particles with the polymer matrix.

Furthermore, the FA particles' hardness gets affected by the crystalline phase of the FA particles since the last enjoy better hardness characteristics.

3.2.3 Polymer-FA composite in FFF

The incorporation of FFF in ABS-FA composite has not been investigated yet. To our knowledge, no one has already added FA particles into ABS for FFF. This study aims to investigate the effects of the utilization of the FA particles on the mechanical properties of the ABS-FA composite FFF-printed parts. The tensile test has performed on the printed specimens to study the composite specimens' mechanical properties comprehensively. The mechanical properties investigated in this study were elastic modulus, yield strength and strain, and fracture strength and strain. Furthermore, differential scanning calorimetry (DSC), thermal gravimetric analysis (TGA), X-ray diffraction analysis (XRD), and scanning electron microscopy (SEM) have been performed for comprehensive analysis of the thermal, structural and mechanical behaviour of the printed parts.

3.3 Experimental details

An open source Flashforge Pro 3D printer printed all the dog-bone shaped specimens.

3.3.1 Pure ABS and ABS-FA Filament preparation

FA particles were obtained from a commercial coal power plant in Turkey. The FA was sieved by a 75 μm mesh to eliminate the larger particles. The sieved FA was dried in an oven at 70°C for 3 hours before mixing.; Figure 23 shows an SEM image of the FA particles used in this study and the size distribution of the particles.

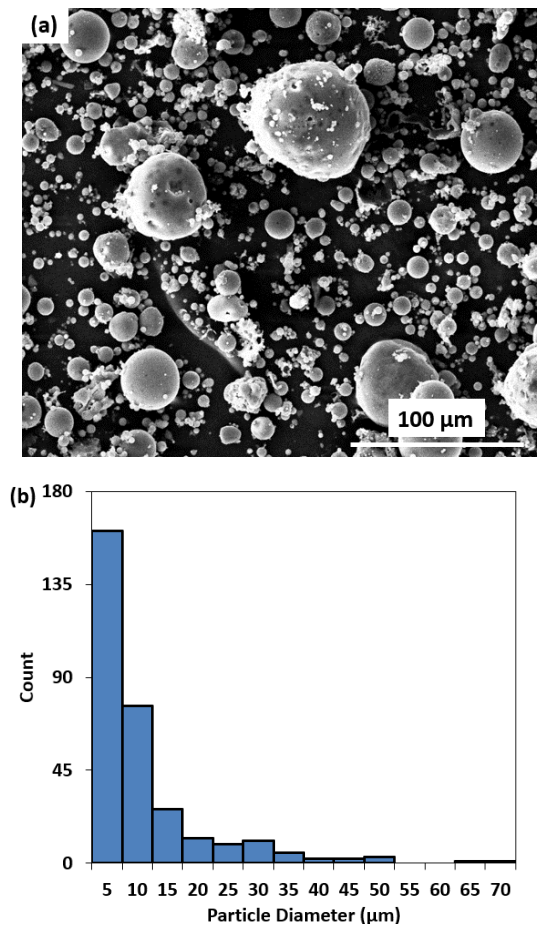


Figure 23. (a) SEM image of the FA used in this study and (b) particle size distribution histogram.

Novodur HD M203FC ABS pellets were purchased from Ineos Styrolution (Germany) and were dried at 60 °C for 4 hours before mixing. A Thermoprism TSE-16-TC twin-screw extruder (L/D = 24) with a co-rotating screw configuration mixed ABS with the FA particles and produced the filaments with 2 wt.% FA. The screw speed was 30 rpm, and the five-stage temperature profile from hopper to die was 190°C – 230°C – 230°C – 235°C – 240°C, respectively. The extruded filament was cut into small pieces and extruded again to obtain better homogeneity and a more accurate filament diameter. Several measurements over the length of the filament yielded an average diameter of 1.75 ± 15 mm. The same conditions were used for extruding the pure ABS filament.

I printed all the dog bone-shaped specimens, Figure 24 (a), for the tensile test based on the ASTM D638-4 Standard Test Method for Tensile Properties of Plastics, considering five identical specimens for the pure ABS and ABS-FA composite filaments. Table 11 summarizes the printing parameters that are common to all specimens of this study.

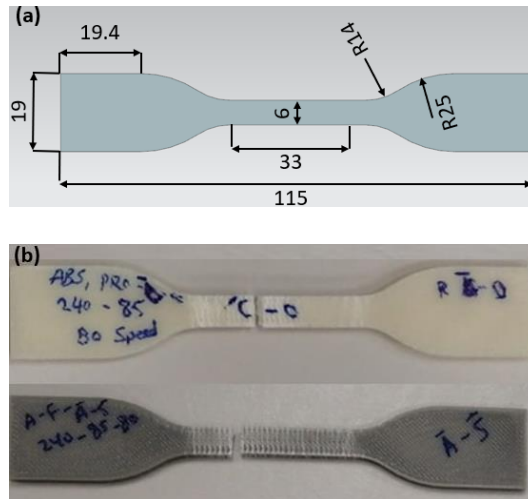


Figure 24. (a) Dimensions of the tensile specimen. The specimen thickness is 3.2 mm. (b) Photographs of tested specimens of the pure ABS (white) and the ABS-FA (grey).

Table 11. The printing parameters common to all specimens of this study.

Layer thickness (mm)	0.2
Printing speed (mm/s)	80
Infill density (%), Pattern	100 (Lines)
Infill Line Directions	± 45
Nozzle diameter (mm)	0.4
Nozzle temperature ($^{\circ}\text{C}$)	240
Bed temperature ($^{\circ}\text{C}$)	80

3.3.2 Mechanical testing

The universal testing machine Zwick/Roell (Z250), Germany, performed the tensile test at room temperature with a 20 mm/min displacement rate. To get a clear insight on the effect of the addition of FA particles on the mechanical properties of ABS, I investigated, in a systematic way, the change in elastic modulus, yield, and fracture properties.

3.3.3 Surface morphology characterization

An FEI QUANTA 400F field-emission SEM (Hillsboro, Oregon) examined both the distribution of FA in ABS and the fracture morphology of the tested specimens. The specimens were coated with 10 nm Au-Pd before imaging.

3.3.4 X-ray diffraction analysis

A Rigaku Ultima Diffractometer performed X-ray diffraction analysis on the specimens over the 2θ range of $5 - 40^\circ$, at a scanning speed of $2^\circ/\text{min}$.

3.3.5 Differential scanning calorimetry and thermal gravimetric analysis

A Perkin Elmer Pyris 1 (USA) performed thermogravimetric analysis (TGA); the pure specimen and composite specimen were heated in the range between $25-750^\circ\text{C}$ with a heating rate of $10^\circ\text{C}/\text{min}$ in a pure nitrogen atmosphere to prevent degradation. A TA instrument DSC 250 (USA) performed differential scanning calorimetry (DSC) on the specimens. I heated the pure specimen and composite specimen in the range between $50-250^\circ\text{C}$. The heating rate used was at $10^\circ\text{C}/\text{min}$ in a pure nitrogen atmosphere to prevent degradation.

3.4 Results and discussion

3.4.1 XRD results

Figure 25 shows the XRD results of ABS and ABS-FA samples. Pure ABS has a broad peak at $2\theta = 19.5^\circ$. This wide peak and the shoulder at around 13.5° are in agreement with the previous measurements on ABS samples (Wang et al. 2014). The large full width at half maximum is indicative of the amorphous structure of ABS. ABS-FA sample shows an almost identical XRD spectrum, indicating that FA particles are well dispersed and the low FA loading does not influence the amorphous character of the polymer. The data do not exhibit any reflections from the crystal phases of the FA either. I attribute this to the low volume fraction of FA and the detection limit of XRD measurements.

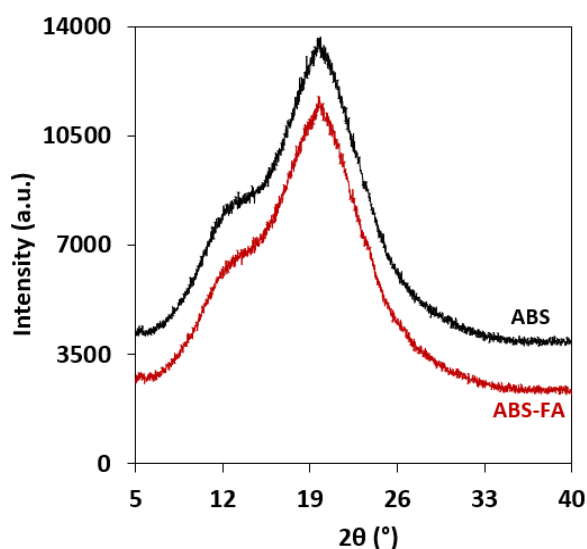


Figure 25. XRD spectrum of pure ABS and ABS-FA composite specimens.

3.4.2 DSC and TGA results

Figure 26 (a) shows the DSC results of ABS and ABS-FA specimens. For pure ABS, the results indicate a glass transition temperature (T_g) of 100°C and a broad endothermic peak around 200°C . These results are in agreement with the literature,

reporting T_g values and broad endothermic transition values around 103 – 107°C, and 210 – 260°C, respectively (Billah et al. 2020; Oral, Ersoy, and Serhatli 2018; Wypych 2016). Being an amorphous polymer, ABS does not exhibit a melting temperature. Therefore, the endotherm present at around 200°C is indicative of the melting or transformation of some constituents of ABS (Billah et al. 2020). The addition of FA particles has no significant effect on the DSC response, apart from a small shift in the glass temperature to 104 °C. This shift might be due to the reduced chain mobility of the polymer, delaying the transition (Billah et al. 2020).

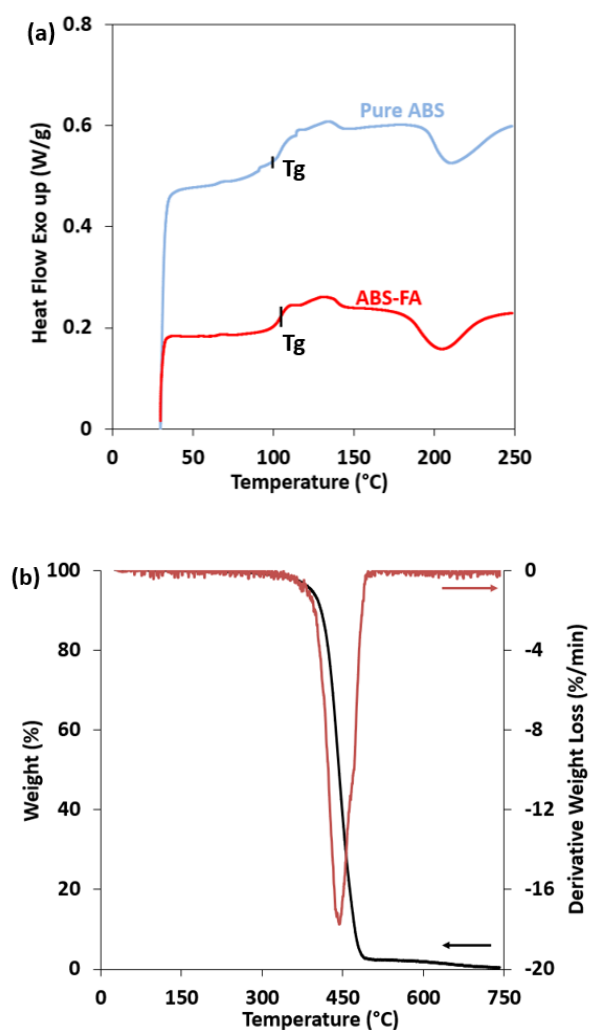


Figure 26. (a) DSC data of ABS and ABS-FA. (b) TGA data of ABS and ABS-FA.

On the other hand, Figure 26 (b) shows the TGA results of the samples. Overall, the results for ABS and ABS-FA are virtually the same, and the data of ABS is omitted for clarity. Pyrolysis takes place at 500°C with a loss of 99% of the weight. The derivative of the TGA curve indicates an inflection point (first derivative peak) of 454 °C for both specimens, which defines the temperature of maximum weight loss rate. Previous studies show that higher FA loading can improve the composite's thermal stability due to the high degradation property of the FA compared with the polymer. The addition of 30 wt.% FA to ABS decreases the loss of weight by 25 % compared to the neat ABS (Bonda et al. 2012). However, the almost identical results in our case are attributed to the low volume fraction of the FA.

3.4.3 Mechanical test results

Figure 27 shows the stress-strain response of ABS and ABS-FA specimens. The results are consistent, demonstrating the repeatability of the printing and the testing procedures.

Table 12 shows the summary of the results. ABS has a fracture strength of about 32 MPa and an elastic modulus of 2 GPa. Previous measurements on FFF-produced ABS specimens indicate a strength and modulus values in a wide range of 2.6-53 MPa and 1.5 – 2.2 GPa, respectively (Ahn et al. 2002; Bakır et al. 2021b; Banjanin et al. 2018), showing that our findings are in general agreement with previous data. The wide range of values in the literature is due to the strong effect of process parameters such as nozzle temperature, raster orientation, and built orientation on the mechanical properties, a phenomenon also observed for other filament materials such as PLA and PET (Bakır et al. 2021a; Kaygusuz and Özerinç 2019). The alternating raster angle of $\pm 45^\circ$ employed in this study is one of the most effective raster patterns that provide a relatively isotropic and strong structure. Nevertheless, the strength of the specimens of this study is lower than that of ABS produced by injection molding, exhibiting values in the range of 40 – 50 MPa (Chen et al. 2007; Rahimi, Esfahanian, and Moradi 2014).

The addition of FA to ABS does not alter the mechanical properties significantly, with the exception of elongation at break. There exists an approximately 50% reduction in elongation at break values with the addition of the FA particles. The primary reason for the reduction in ductility is the restricted chain mobility of the polymer by the presence of the second phase. Previous work shows that surface-modified FA particles can minimize this effect; a ductility reduction of only 24% was reported at an FA loading of 30 wt.% (Bonda et al. 2012). Surface-modified FA provides this improvement by generating a better interfacial adhesion between the ABS matrix and the FA particles (Bonda et al. 2012). This results in a more efficient stress and strain compatibility between the two phases and reduces the stress concentrations due to the shearing at the interface. The analysis results show that there is a need to increase the weight fraction of FA to obtain more significant improvements in the mechanical properties. In our case, increasing the fraction of FA resulted in very brittle filaments causing frequent clogging of the printing head. A possible solution to this problem is using plasticizers to improve the rheological characteristics of the filament.

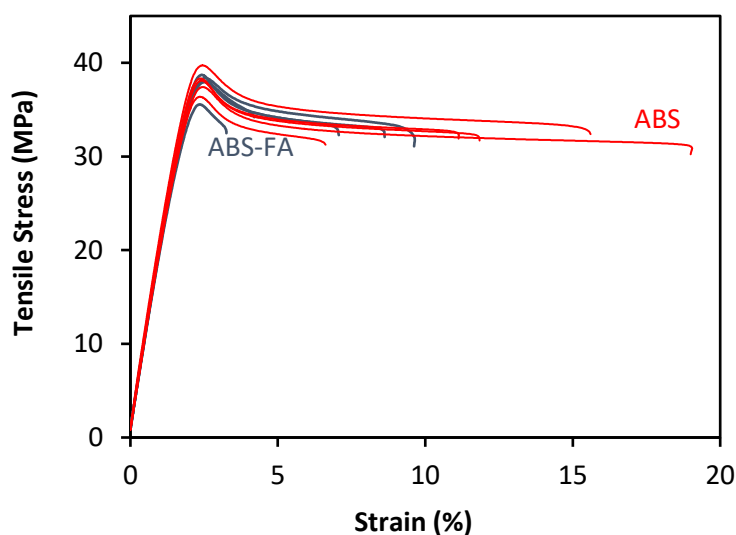


Figure 27. The stress-strain curves for the ABS (red) and ABS-FA (blue) specimens.

Table 12. Summary of the mechanical properties of ABS and ABS-FA specimens.

Material	Elastic Modulus (GPa)	Yield Strength (MPa)	Yield Strain (%)	Fracture Strength (MPa)	Fracture Strain (%)
ABS-FA	2.0±0.1	37.7±1.2	2.4±0.0	32.7±0.8	6.5±2.7
ABS	2.0±0.0	37.9±1.1	2.4±0.1	31.8±0.8	12.8±4.6

Figure 28 shows an SEM image of the fracture surfaces of an ABS-FA specimen. Figure 28 (a) exhibits micron-sized gaps in the polymer matrix. These defects, attributed to the relatively poor rheological characteristics of the filament, act as stress concentration sites leading to premature failure. The close-up view Figure 28 (b) shows several FA particles, demonstrating the weak bonding between the FA particles and the ABS matrix, which constitutes another reason for the poor ductility.

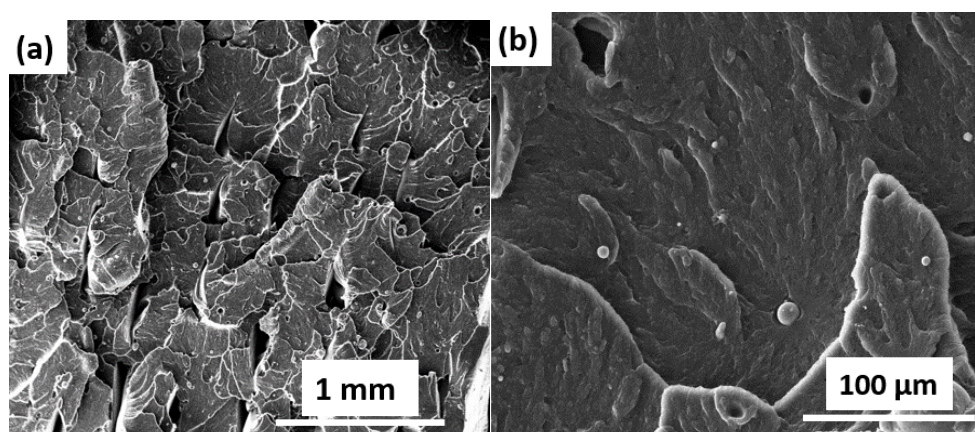


Figure 28. SEM images of the fracture surface of the ABS-FA specimen. (a) and (b) show two different regions of the same surface at different magnifications.

CHAPTER 4

CONCLUSION AND FUTURE WORK

One of the most powerful advantages of FFF is the wide range of applications that can be used for. One of these applications is investigating the applicability of adding a filler into a pure polymer to improve some final properties of the composite. The importance of utilizing composite has led to producing parts with superior final properties that can be used for extremely critical situations. FFF provides an easy way of prototyping applications with low cost and compatible surface quality that can be used to investigate the final properties of the printed parts. Another powerful tool of FFF is the ability to control the printing parameters to tune the final properties of the printed parts to serve a specific purpose.

The first part in this thesis carried out to investigate LW-PLA 3D printed parts' mechanical properties under different printing parameters shows that the nozzle temperature, flow rate, and infill ratio have more significant effects on the mechanical properties compared to the printing speed and the layer thickness, I can summarize my findings as follow;

- Increasing the nozzle temperature from 215 - 260 °C deteriorates the mechanical properties by a factor of 2.5. High nozzle temperature leads to more foams that occupy the melted material leading to a fragile structure.
- A lower flow rate leads to more small foams inside the printed parts, which in turn leads to more thin, fragile walls and eventually faster failure.
- As the specimen infill ratio increases, the load-bearing capacity will increase since the thickness of the walls surrounding the empty spaces will increase leading to better strength properties.

- The printing speed and the layer thickness are more related to the surface quality and the printing time. However, these parameters should be adjusted carefully for better surface properties.

In general, the printing parameters significantly affect the mechanical properties of 3D printed parts, and to get the desired properties, an excellent optimization of these parameters should be achieved.

Although foamed PLA polymer is a promising material that can be used especially in medical and energy absorbing applications, its low mechanical properties should get more attention in future research. Different technologies can be used to improve this foaming polymer's strength; improving its low melt properties can be considered as a promising method.

The second part of this thesis investigated FFF-produced ABS and ABS-FA specimens' structural, thermal, and mechanical properties. The thermal and mechanical properties of the composite did not change significantly by the addition of 2 wt.% FA. The only exception was a drastic decrease in ductility by a factor of two upon FA additions. The maintained properties of ABS-FA can be considered as an indication of the feasibility of FA additions to ABS filament, especially for coloring applications. On the other hand, for achieving any improvement in the mechanical properties through the same route, I propose the following steps for future work:

- Using surface-modified FA particles can enhance the structural integrity of the composite. Silane coupling agent treatment compatible with the polymer matrix can be a good choice for this purpose, effectively improving the interfacial adhesion between the FA and the polymer matrix.
- Increasing the FA loading to beyond 10 wt.% and utilizing a suitable plasticizer can provide strengthening and defect-free printed structures at the same time.

REFERENCES

- Abeykoon, Chamil, Pimpisut Sri-Amphorn, and Anura Fernando. 2020. "Optimization of Fused Deposition Modeling Parameters for Improved PLA and ABS 3D Printed Structures." *International Journal of Lightweight Materials and Manufacture* 3(3):284–97. doi: 10.1016/j.ijlmm.2020.03.003.
- ACAA. n.d. "The American Coal Ash Association." Retrieved January 3, 2021 (https://www.acaa-usa.org/Portals/9/Files/PDFs/2010_CCP_Survey_FINAL_102011.pdf).
- Ahmaruzzaman, M. 2010. "A Review on the Utilization of Fly Ash." *Progress in Energy and Combustion Science* 36(3):327–63.
- Ahn, Sung Hoon, Michael Montero, Dan Odell, Shad Roundy, and Paul K. Wright. 2002. "Anisotropic Material Properties of Fused Deposition Modeling ABS." *Rapid Prototyping Journal* 8(4):248–57. doi: 10.1108/13552540210441166.
- Akın, Süleyman Şener, Duarte Magalhães, and Feyza Kazanç. 2020. "A Study on the Effects of Various Combustion Parameters on the Mineral Composition of Tunçbilek Fly Ash." *Fuel* 275:117881. doi: 10.1016/j.fuel.2020.117881.
- Aliheidari, Nahal, Rajasekhar Tripuraneni, Cameron Hohimer, Josef Christ, Amir Ameli, and Siva Nadimpalli. 2017. "The Impact of Nozzle and Bed Temperatures on the Fracture Resistance of FDM Printed Materials." P. 1016512 in *Behavior and Mechanics of Multifunctional Materials and Composites 2017*. Vol. 10165. SPIE.
- Anitha, R., S. Arunachalam, and P. Radhakrishnan. 2001. "Critical Parameters Influencing the Quality of Prototypes in Fused Deposition Modelling." Pp. 385–88 in *Journal of Materials Processing Technology*. Vol. 118. Elsevier.
- Anon. 2002. "ACI PRC-232.2-18: Report on the Use of Fly Ash in Concrete. American Concrete Institute, USA."
- Atikler, U., D. Basalp, and F. Tihminlioğlu. 2006. "Mechanical and Morphological Properties of Recycled High-Density Polyethylene, Filled with Calcium Carbonate and Fly Ash." *Journal of Applied Polymer Science* 102(5):4460–67. doi: 10.1002/app.24772.
- Ayrilmis, Nadir. 2018. "Effect of Layer Thickness on Surface Properties of 3D Printed Materials Produced from Wood Flour/PLA Filament." *Polymer Testing* 71:163–66. doi: 10.1016/j.polymertesting.2018.09.009.
- Bakır, Ali Alperen, Resul Atik, and Sezer Özerinç. 2021a. "Effect of Fused Deposition Modeling Process Parameters on the Mechanical Properties of Recycled Polyethylene Terephthalate Parts." *Journal of Applied Polymer*

Science 138(3). doi: 10.1002/app.49709.

- Bakır, Ali Alperen, Resul Atik, and Sezer Özerinç. 2021b. “Mechanical Properties of Thermoplastic Parts Produced by Fused Deposition Modeling: A Review.” *Rapid Prototyping Journal*.
- Banjanin, Bojan, Gojko Vladić, Magdolna Pál, Sebastian Baloš, Miroslav Dramićanin, Milan Rackov, and Ivan Knežević. 2018. “Consistency Analysis of Mechanical Properties of Elements Produced by FDM Additive Manufacturing Technology.” *Revista Materia* 23(4). doi: 10.1590/s1517-707620180004.0584.
- Basu, Arijit, Michael Nazarkovsky, Rohan Ghadi, Wahid Khan, and Abraham J. Domb. 2017. “Poly(Lactic Acid)-Based Nanocomposites.” *Polymers for Advanced Technologies* 28(8):919–30.
- Billah, Kazi Md Masum, Fernando A. R. Lorenzana, Nikki L. Martinez, Ryan B. Wicker, and David Espalin. 2020. “Thermomechanical Characterization of Short Carbon Fiber and Short Glass Fiber-Reinforced ABS Used in Large Format Additive Manufacturing.” *Additive Manufacturing* 35. doi: 10.1016/j.addma.2020.101299.
- Bishop, R. E., and R. J. Smallman. 2002. “Materials for Sports.” *Chemical and Engineering News* 80(5):29. doi: 10.1016/b978-075064564-5/50014-8.
- Blissett, R. S., and N. A. Rowson. 2012. “A Review of the Multi-Component Utilisation of Coal Fly Ash.” *Fuel* 97:1–23.
- Bonda, Sateesh, Smita Mohanty, and Sanjay K. Nayak. 2012. “Viscoelastic, Mechanical, and Thermal Characterization of Fly Ash-Filled ABS Composites and Comparison of Fly Ash Surface Treatments.” *Polymer Composites* 33(1):22–34. doi: 10.1002/pc.21242.
- Bonda, Sateesh, Smita Mohanty, and Sanjay Kumar Nayak. 2016. “Property Evaluation of Nanostructured Fly Ash-Reinforced Acrylonitrile Butadiene Styrene Nanocomposites.” *Journal of Thermoplastic Composite Materials* 29(12):1611–26. doi: 10.1177/0892705715569828.
- Branciforti, Marcia Cristina, Tassiana Araujo Custodio, Lilia Muller Guerrini, Luc Avérous, Rosario Elida, and Suman Bretas. 2009. “Characterization of Nano-Structured Poly(D,L-Lactic Acid) Nonwoven Mats Obtained from Different Solutions by Electrospinning.” *Journal of Macromolecular Science, Part B* 48(6):1222–40. doi: 10.1080/10408390903060970.
- Calvert, Kayla L., Kevin P. Trumble, Thomas J. Webster, and Lynn A. Kirkpatrick. 2010. “Characterization of Commercial Rigid Polyurethane Foams Used as Bone Analogs for Implant Testing.” *Journal of Materials Science: Materials in Medicine* 21(5):1453–61. doi: 10.1007/s10856-010-4024-6.
- Chacón, J. M., M. A. Caminero, E. García-Plaza, and P. J. Núñez. 2017. “Additive

- Manufacturing of PLA Structures Using Fused Deposition Modelling: Effect of Process Parameters on Mechanical Properties and Their Optimal Selection.” *Materials and Design* 124:143–57. doi: 10.1016/j.matdes.2017.03.065.
- Chartier, Thierry, and Alexander Badev. 2013. “Rapid Prototyping of Ceramics.” Pp. 489–524 in *Handbook of Advanced Ceramics: Materials, Applications, Processing, and Properties: Second Edition*. Elsevier Inc.
- Chen, Chun Sheng, Tsyr Jang Chen, Rean Der Chien, and Shia Chung Chen. 2007. “Investigation on the Weldline Strength of Thin-Wall Injection Molded ABS Parts.” *International Communications in Heat and Mass Transfer* 34(4):448–55. doi: 10.1016/j.icheatmasstransfer.2007.01.005.
- Choi, Won Jun, Ki Seob Hwang, Hyuk Jun Kwon, Chanmin Lee, Chae Hwa Kim, Tae Hee Kim, Seung Won Heo, Jung Hyun Kim, and Jun Young Lee. 2020. “Rapid Development of Dual Porous Poly(Lactic Acid) Foam Using Fused Deposition Modeling (FDM) 3D Printing for Medical Scaffold Application.” *Materials Science and Engineering C* 110:110693. doi: 10.1016/j.msec.2020.110693.
- Chou, Mei-In Melissa. 2012. “Fly Ash .” Pp. 3820–43 in *Encyclopedia of Sustainability Science and Technology*. Springer New York.
- Colorfabb. n.d. “Low Density PLA (LW-PLA).” Retrieved (<https://learn.colorfabb.com/lw-pla/>).
- Deepthi, M. V., Madan Sharma, R. R. N. Sailaja, P. Anantha, P. Sampathkumaran, and S. Seetharamu. 2010. “Mechanical and Thermal Characteristics of High Density Polyethylene-Fly Ash Cenospheres Composites.” *Materials and Design* 31(4):2051–60. doi: 10.1016/j.matdes.2009.10.014.
- Deng, Xiaohu, Zhi Zeng, Bei Peng, Shuo Yan, and Wenchao Ke. 2018. “Mechanical Properties Optimization of Poly-Ether-Ether-Ketone via Fused Deposition Modeling.” *Materials* 11(2):216. doi: 10.3390/ma11020216.
- Dromel, Pierre C., and Deepti Singh. 2021. “Biomanufacturing.” Pp. 137–70 in *3D Printing in Medicine and Surgery*. Elsevier.
- Dwivedi, Aakash, and M. Jain. 2014. “Fly Ash – Waste Management and Overview : A Review.” *Undefined*.
- Eirich, F. R. 1978. “Handbook of Fillers and Reinforcements for Plastics, Harry S. Katz and John V. Milewski, Eds., Van Nostrand Reinhold, New York, 1978, 652 Pp., \$44.95.” *Journal of Polymer Science: Polymer Letters Edition* 16(10):551–551. doi: 10.1002/pol.1978.130161012.
- Farah, Shady, Daniel G. Anderson, and Robert Langer. 2016. “Physical and Mechanical Properties of PLA, and Their Functions in Widespread Applications — A Comprehensive Review.” *Advanced Drug Delivery*

Reviews 107:367–92.

- Fountas, Nikolaos A., and Nikolaos M. Vaxevanidis. 2021. “Optimization of Fused Deposition Modeling Process Using a Virus-Evolutionary Genetic Algorithm.” *Computers in Industry* 125. doi: 10.1016/j.compind.2020.103371.
- Garlotta, Donald. 2001. “A Literature Review of Poly(Lactic Acid).” *Journal of Polymers and the Environment* 9(2):63–84. doi: 10.1023/A:1020200822435.
- Gibson, Lorna J., and Michael F. Ashby. 1997. *Cellular Solids*. Cambridge University Press.
- Gollakota, Anjani R. K., Vikranth Volli, and Chi Min Shu. 2019. “Progressive Utilisation Prospects of Coal Fly Ash: A Review.” *Science of the Total Environment* 672:951–89.
- Guessasma, Sofiane, Sofiane Belhabib, and Hedi Nouri. 2021. “Effect of Printing Temperature on Microstructure, Thermal Behavior and Tensile Properties of 3D Printed Nylon Using Fused Deposition Modeling.” *Journal of Applied Polymer Science* 138(14). doi: 10.1002/app.50162.
- Guhanathan, S., and M. Saroja Devi. 2004. “Studies on Interface in Polyester/Fly-Ash Particulate Composites.” *Composite Interfaces* 11(1):43–66. doi: 10.1163/156855404322681046.
- Iyer, R. S., and J. A. Scott. 2001. “Power Station Fly Ash - A Review of Value-Added Utilization Outside of the Construction Industry.” *Resources, Conservation and Recycling* 31(3):217–28. doi: 10.1016/S0921-3449(00)00084-7.
- Joshi, R. 1997. *Fly Ash in Concrete : Production, Properties and Uses*. Amsterdam: Gordon and Breach Science Publishers.
- K. Wesche. 1991. *Fly Ash in Concrete: Properties and Performance*. CRC Press.
- Kaygusuz, Burçin, and Sezer Özerinç. 2019. “Improving the Ductility of Polylactic Acid Parts Produced by Fused Deposition Modeling through Polyhydroxyalkanoate Additions.” *Journal of Applied Polymer Science* 136(43):48154. doi: 10.1002/app.48154.
- Khodaei, Mohammad, Kamran Amini, and Alireza Valanezhad. 2020. “Fabrication and Characterization of Poly Lactic Acid Scaffolds by Fused Deposition Modeling for Bone Tissue Engineering.” *Journal Wuhan University of Technology, Materials Science Edition* 35(1):248–51. doi: 10.1007/s11595-020-2250-4.
- Li, L., and Q. Sun. 2008. “Composite Modeling and Analysis for Fabrication of FDM Prototypes with Locally Controlled Properties.”
- Li, R., K. L. Chen, Y. Wang, Y. S. Liu, Y. S. Zhou, and Y. C. Sun. 2019. “Establishment of a 3D Printing System for Bone Tissue Engineering Scaffold

- Fabrication and the Evaluation of Its Controllability over Macro and Micro Structure Precision.” *Beijing Da Xue Xue Bao. Yi Xue Ban = Journal of Peking University. Health Sciences* 51(1):115–19. doi: 10.19723/j.issn.1671-167X.2019.01.021.
- Lim, L. T., R. Auras, and M. Rubino. 2008. “Processing Technologies for Poly(Lactic Acid).” *Progress in Polymer Science (Oxford)* 33(8):820–52.
- Liu, Zhaobing, Qian Lei, and Shuaiqi Xing. 2019. “Mechanical Characteristics of Wood, Ceramic, Metal and Carbon Fiber-Based PLA Composites Fabricated by FDM.” *Journal of Materials Research and Technology* 8(5):3743–53. doi: 10.1016/j.jmrt.2019.06.034.
- Matsunaga, T., J. K. Kim, S. Hardcastle, and P. K. Rohatgi. 2002. “Crystallinity and Selected Properties of Fly Ash Particles.” *Materials Science and Engineering A* 325(1–2):333–43. doi: 10.1016/S0921-5093(01)01466-6.
- Matsuzaki, Ryosuke, Masahito Ueda, Masaki Namiki, Tae Kun Jeong, Hirosuke Asahara, Keisuke Horiguchi, Taishi Nakamura, Akira Todoroki, and Yoshiyasu Hirano. 2016. “Three-Dimensional Printing of Continuous-Fiber Composites by in-Nozzle Impregnation.” *Scientific Reports* 6(1):1–7. doi: 10.1038/srep23058.
- Mohan, N., P. Senthil, S. Vinodh, and N. Jayanth. 2017. “A Review on Composite Materials and Process Parameters Optimisation for the Fused Deposition Modelling Process.” *Virtual and Physical Prototyping* 12(1):47–59.
- Moura, Nayara Koba de, Idália A. W. B. Siqueira, João Paulo de Barros Machado, Hueliton Wilian Kido, Ingrid Regina Avanzi, Ana Claudia Muniz Rennó, Eliandra de Sousa Trichês, and Fabio Roberto Passador. 2019. “Production and Characterization of Porous Polymeric Membranes of PLA/PCL Blends with the Addition of Hydroxyapatite.” *Journal of Composites Science* 3(2):45. doi: 10.3390/jcs3020045.
- Nikzad, M., S. H. Masood, and I. Sbarski. 2011. “Thermo-Mechanical Properties of a Highly Filled Polymeric Composites for Fused Deposition Modeling.” *Materials and Design* 32(6):3448–56. doi: 10.1016/j.matdes.2011.01.056.
- de Oliveira, Grasielli C., Lucas C. Pereira, Ana L. Silva, Felipe S. Semaan, Marilza Castilho, and Eduardo A. Ponzio. 2018. “Acrylonitrile-Butadiene-Styrene (ABS) Composite Electrode for the Simultaneous Determination of Vitamins B2 and B6 in Pharmaceutical Samples.” *Journal of Solid State Electrochemistry* 22(5):1607–19. doi: 10.1007/s10008-018-3897-z.
- Olivera, Sharon, Handanahally Basavarajaiah Muralidhara, Krishna Venkatesh, Keshavanarayana Gopalakrishna, and Chinnaganahalli Suryaprakash Vivek. 2016. “Plating on Acrylonitrile–Butadiene–Styrene (ABS) Plastic: A Review.” *Journal of Materials Science* 51(8):3657–74.

- Omnexus. n.d. "Acrylonitrile Butadiene Styrene (ABS) and Its Features."
- Oral, Mehmet A., Osman G. Ersoy, and Ersin Serhatli. 2018. "Effect of Acrylonitrile–Butadiene–Styrene/Polyethylene Terephthalate Blends on Dimensional Stability, Morphological, Physical and Mechanical Properties and after Aging at Elevated Temperature." *Journal of Plastic Film and Sheeting* 34(4):394–417. doi: 10.1177/8756087918768348.
- Pardo, S. G., C. Bernal, A. Ares, M. J. Abad, and J. Cano. 2010. "Rheological, Thermal, and Mechanical Characterization of Fly Ash-Thermoplastic Composites with Different Coupling Agents." *Polymer Composites* 31(10):1722–30. doi: 10.1002/pc.20962.
- Rahimi, Mohammad, Mohsen Esfahanian, and Mehran Moradi. 2014. "Effect of Reprocessing on Shrinkage and Mechanical Properties of ABS and Investigating the Proper Blend of Virgin and Recycled ABS in Injection Molding." *Journal of Materials Processing Technology* 214(11):2359–65. doi: 10.1016/j.jmatprotec.2014.04.028.
- Ramlan, M. I. S., and N. A. Shuaib. 2018. "Environmental Assessment and Mechanical Properties of Acrylonitrile Butadiene Styrene (ABS) Reinforced with Fly Ash Filler." P. 020018 in *AIP Conference Proceedings*. Vol. 2030. American Institute of Physics Inc.
- Ramsteiner, F., N. Fell, and S. Forster. 2001. "Testing the Deformation Behaviour of Polymer Foams." *Polymer Testing* 20(6):661–70. doi: 10.1016/S0142-9418(00)00090-8.
- Samykan, M., S. K. Selvamani, K. Kadirgama, W. K. Ngui, G. Kanagaraj, and K. Sudhakar. 2019. "Mechanical Property of FDM Printed ABS: Influence of Printing Parameters." *International Journal of Advanced Manufacturing Technology* 102(9–12):2779–96. doi: 10.1007/s00170-019-03313-0.
- Sanz-Horta, Raúl, Carlos Elvira, Alberto Gallardo, Helmut Reinecke, and Juan Rodríguez-Hernández. 2020. "Fabrication of 3D-Printed Biodegradable Porous Scaffolds Combining Multi-Material Fused Deposition Modeling and Supercritical CO₂ Techniques." *Nanomaterials* 10(6):1080. doi: 10.3390/nano10061080.
- Satheesh Raja, R., K. Manisekar, and V. Manikandan. 2014. "Study on Mechanical Properties of Fly Ash Impregnated Glass Fiber Reinforced Polymer Composites Using Mixture Design Analysis." *Materials and Design* 55:499–508. doi: 10.1016/j.matdes.2013.10.026.
- Singh, Daljeet, Atul Babbar, Vivek Jain, Dheeraj Gupta, Sanjai Saxena, and Vagish Dwivedi. 2019. "Synthesis, Characterization, and Bioactivity Investigation of Biomimetic Biodegradable PLA Scaffold Fabricated by Fused Filament Fabrication Process." *Journal of the Brazilian Society of Mechanical Sciences and Engineering* 41(3):121. doi: 10.1007/s40430-019-1625-y.

- Sreekanth, M. S., V. A. Bambole, S. T. Mhaske, and P. A. Mahanwar. 2009. *Effect of Particle Size and Concentration of Flyash on Properties of Polyester Thermoplastic Elastomer Composites*. Vol. 8.
- Sun, Xuemei, Hao Sun, Houpu Li, and Huisheng Peng. 2013. "Developing Polymer Composite Materials: Carbon Nanotubes or Graphene?" *Advanced Materials* 25(37):5153–76.
- Tekinalp, Halil L., Vlastimil Kunc, Gregorio M. Velez-Garcia, Chad E. Duty, Lonnie J. Love, Amit K. Naskar, Craig A. Blue, and Soydan Ozcan. 2014. "Highly Oriented Carbon Fiber-Polymer Composites via Additive Manufacturing." *Composites Science and Technology* 105:144–50. doi: 10.1016/j.compscitech.2014.10.009.
- Torres, Jonathan, Matthew Cole, Allen Owji, Zachary DeMastry, and Ali P. Gordon. 2016. "An Approach for Mechanical Property Optimization of Fused Deposition Modeling with Polylactic Acid via Design of Experiments." *Rapid Prototyping Journal* 22(2):387–404. doi: 10.1108/RPJ-07-2014-0083.
- Uddin, M. S., M. F. R. Sidek, M. A. Faizal, Reza Ghomashchi, and A. Pramanik. 2017. "Evaluating Mechanical Properties and Failure Mechanisms of Fused Deposition Modeling Acrylonitrile Butadiene Styrene Parts." *Journal of Manufacturing Science and Engineering, Transactions of the ASME* 139(8). doi: 10.1115/1.4036713.
- Valerga Puerta, Ana P., S. R. Fernandez-Vidal, Moises Batista, and F. Girot. 2019. "Fused Deposition Modelling Interfacial and Interlayer Bonding in PLA Post-Processed Parts." *Rapid Prototyping Journal* 26(3):585–92. doi: 10.1108/RPJ-06-2019-0176.
- Wach, Radoslaw A., Piotr Wolszczak, and Agnieszka Adamus-Wlodarczyk. 2018. "Enhancement of Mechanical Properties of FDM-PLA Parts via Thermal Annealing." *Macromolecular Materials and Engineering* 303(9):1800169. doi: 10.1002/mame.201800169.
- Wampol, Calvin. 2018. "Additive Manufacturing with High Density Polyethylene: Mechanical Properties Evaluation." South Dakota State University.
- Wang, Xin, Man Jiang, Zuowan Zhou, Jihua Gou, and David Hui. 2017. "3D Printing of Polymer Matrix Composites: A Review and Prospective." *Composites Part B: Engineering* 110:442–58.
- Wang, Zongyuan, Jiajun Wang, Minyue Li, Kaihang Sun, and Chang Jun Liu. 2014. "Three-Dimensional Printed Acrylonitrile Butadiene Styrene Framework Coated with Cu-BTC Metal-Organic Frameworks for the Removal of Methylene Blue." *Scientific Reports* 4(1):1–7. doi: 10.1038/srep05939.
- Weng, Zixiang, Jianlei Wang, T. Senthil, and Lixin Wu. 2016. "Mechanical and

- Thermal Properties of ABS/Montmorillonite Nanocomposites for Fused Deposition Modeling 3D Printing.” *Materials and Design* 102:276–83. doi: 10.1016/j.matdes.2016.04.045.
- Wimpenny, David Ian., Pulak M. Pandey, and L. Jyothish. Kumar. 2017. *Advances in 3D Printing & Additive Manufacturing Technologies*.
- Wu, Ningjing, and Xiangting Li. 2014. “Flame Retardancy and Synergistic Flame Retardant Mechanisms of Acrylonitrile-Butadiene-Styrene Composites Based on Aluminum Hypophosphite.” *Polymer Degradation and Stability* 105(1):265–76. doi: 10.1016/j.polymdegradstab.2014.04.011.
- Wypych, George. 2016. *Handbook of Polymers 2nd Edition*.
- Xue, Bai, Jianjun Bao, and Junhua Zhang. 2016. “Ultrafine Fly Ash as a Reinforcing Filler in Poly(Lactic Acid) Matrix.” *Journal of Applied Polymer Science* 133(30). doi: 10.1002/app.43716.
- Yang, Yu Fen, Guo Sheng Gai, Zhen Fang Cai, and Qing Ru Chen. 2006. “Surface Modification of Purified Fly Ash and Application in Polymer.” *Journal of Hazardous Materials* 133(1–3):276–82. doi: 10.1016/j.jhazmat.2005.10.028.
- Yao, Z. T., M. S. Xia, P. K. Sarker, and T. Chen. 2014. “A Review of the Alumina Recovery from Coal Fly Ash, with a Focus in China.” *Fuel* 120:74–85.
- Zandi, M. Damous, Ramon Jerez-Mesa, Jordi Lluma-Fuentes, Jordi Jorba-Peiro, and J. Antonio Travieso-Rodriguez. 2020. “Study of the Manufacturing Process Effects of Fused Filament Fabrication and Injection Molding on Tensile Properties of Composite PLA-Wood Parts.” *International Journal of Advanced Manufacturing Technology* 108(5–6):1725–35. doi: 10.1007/s00170-020-05522-4.
- Zein, Iwan, Dietmar W. Hutmacher, Kim Cheng Tan, and Swee Hin Teoh. 2002. “Fused Deposition Modeling of Novel Scaffold Architectures for Tissue Engineering Applications.” *Biomaterials* 23(4):1169–85. doi: 10.1016/S0142-9612(01)00232-0.
- Zhao, Yachen, Kai Zhao, Yuchan Li, and Fei Chen. 2020. “Mechanical Characterization of Biocompatible PEEK by FDM.” *Journal of Manufacturing Processes* 56:28–42. doi: 10.1016/j.jmapro.2020.04.063.
- Zilberman, Meital. 2005. “Dexamethasone Loaded Bioresorbable Films Used in Medical Support Devices: Structure, Degradation, Crystallinity and Drug Release.” *Acta Biomaterialia* 1(6):615–24. doi: 10.1016/j.actbio.2005.06.007.

APPENDICES

A. Ashby-Gibson Model of Closed-cell Foam Structures

Gibson-Ashby model is able for estimating the relative modulus for closed-cell foam structures,

$$\frac{E_F}{E_S} = \varphi^2 * \left(\frac{\rho_F}{\rho_S}\right)^2 + (1 - \varphi) * \left(\frac{\rho_F}{\rho_S}\right) + \frac{P_0}{E_S} * \frac{(1-2*\nu_F)}{\left(1-\frac{\rho_F}{\rho_S}\right)}$$

Where E, ν , and ρ are the elastic modulus, Poisson's ratio, and density of the material, and P_0 is the pressure of the cell gas. Subscript S and F refer to the fully solid and foamed specimens, respectively. The constant φ represents the struts portion in the foamed material. The third term is neglected since it is much smaller than the other two terms as an order of magnitude.